

İSTANBUL TECHNICAL UNIVERSITY ★ GRADUATE SCHOOL OF SCIENCE
ENGINEERING AND TECHNOLOGY

Impervious Surface Estimation and Mapping via Remotely Sensed Techniques

M.Sc. THESIS

Kaveh Khorshid

Department of Geomatics Engineering

Geomatics Engineering Programme

Thesis Advisor: Assoc. Prof. Dr. Filiz BEKTAS BALCIK

June 2016

İSTANBUL TECHNICAL UNIVERSITY ★ GRADUATE SCHOOL OF SCIENCE
ENGINEERING AND TECHNOLOGY

Impervious Surface Estimation and Mapping via Remotely Sensed Techniques

M.Sc. THESIS

Kaveh KHORSHID
501121615

Department of Geomatics Engineering

Geomatics Engineering Programme

Thesis Advisor: Assoc. Prof. Dr. Filiz BEKTAS BALCIK

June 2016

İSTANBUL TEKNİK ÜNİVERSİTESİ ★ FEN BİLİMLERİ ENSTİTÜSÜ

Uzaktan Algılama Teknikleri İle Geçirimsiz Yüzey Tahmini ve Haritalanması

YÜKSEK LİSANS TEZİ

**Kaveh KHORSHID
501121615**

Geomatik Mühendisliği Anabilim Dalı

Geomatik Mühendisliği Programı

Tez Danışmanı: Doç.Dr. Filiz Bektas BALCIK

Haziran 2016

Kaveh-Khorshid, a **M.Sc** student of **İTU Graduate School of Science Engineering and Technology** student ID **501121615**, successfully defended the thesis entitled **“IMPERVIOUS SURFACE ESTIMATION AND MAPPING VIA REMOTELY SENSED TECHNIQUES”**, which he prepared after fulfilling the requirements specified in the associated legislations, before the jury whose signatures are below.

Thesis Advisor : **Doç.Dr. Filiz Bektas BALCIK**

İstanbul Technical University

Jury Members : **Prof.Dr. Dursun Zafer Seker**

İstanbul Technical University

Prof.Dr. Bulent Bayram

Yildiz Technical University

Date of Submission : 5 May 2016

Date of Defense : 8 June 2016

To my dear family,

FOREWORD

I would like to take this opportunity to thank many people for their support and contribute toward the completion of this dissertation. First, I would like to express my sincere appreciation to my dear advisor, Assoc.Prof.Dr. Filiz bektas BALCIK, for her patience, motivation, enthusiasm, immense knowledge and continuous guidance and support throughout my program of study and this research work.

I would like to thank my father, who that support me not only during my MSc. thesis but also during my whole life. Also I thank my mother for her great love and encouragement. At the end, many thanks to my dear friends for their help and support.

May 2016

Kaveh KHORSHID
(Civil engineer)

TABLE OF CONTENTS

| | <u>Page</u> |
|--|--------------|
| FOREWORD | ix |
| TABLE OF CONTENTS | xi |
| ABBREVIATIONS | xiii |
| LIST OF TABLES | xv |
| LIST OF FIGURES | xvii |
| SUMMARY | xix |
| ÖZET | xxiii |
| 1. INTRODUCTION | 1 |
| 2. ARTIFICIAL SURFACE | 5 |
| 2.1 Artificial Surfaces Defined and Described..... | 5 |
| 2.2 Development of Impervious Surfaces as an Environmental Indicator..... | 6 |
| 3. REMOTE SENSING OF ARTIFICIAL SURFACES | 9 |
| 3.1 Principles of Remote Sensing | 9 |
| 3.2 Electromagnetic Spectrum and Radiation | 10 |
| 3.3 Electromagnetic Interaction with Earth’s Features Spectral Reflectance | 12 |
| 3.3.1 Built up reflectance | 13 |
| 3.4 Techniques for Mapping and Estimating Impervious Surfaces | 16 |
| 3.4.1 Optical surveying and global positioning systems..... | 17 |
| 3.4.2 Photographic interpretation..... | 17 |
| 3.4.3 Detailed maps..... | 17 |
| 3.4.4 Population density..... | 18 |
| 3.4.5 Image classification..... | 18 |
| 4. REMOTE SENSING IMAGE PROCESSING | 21 |
| 4.1 Digital Image..... | 21 |
| 4.2 Remote Sensing Spectral Indices | 21 |
| 4.3 Built-up Indices | 22 |
| 4.3.1 Normalised difference built-up index (NDBI)..... | 23 |
| 4.3.2 Normalized difference bareness index (NDBaI)..... | 24 |
| 4.3.3 Index-based built-up index (IBI)..... | 25 |
| 4.3.4 Urban index (UI)..... | 26 |
| 4.3.5 Enhanced built-up and bareness index (EBBI)..... | 27 |
| 4.4 Image Classification | 28 |
| 4.5 Density Slicing | 29 |
| 4.6 Accuracy Assessment..... | 29 |
| 5. STUDY AREA , DATA AND CASE STUDY | 33 |
| 5.1 Study Area..... | 33 |
| 5.2 Data Used | 35 |
| 5.2.1 Remote sensing satellites | 35 |
| 5.2.2 Landsat system..... | 36 |
| 5.2.3 Characteristics of Landsat..... | 36 |
| 5.2.3.1 Sensors and specifications..... | 36 |

| | |
|---|-----------|
| 5.3 Spectral Indices | 40 |
| 5.3.1 Built-up area indices..... | 40 |
| 5.4 Mapping Impervious Surface and Bare Land..... | 49 |
| 5.5 Accuracy Assessment..... | 54 |
| 6. CONCLUSIONS AND RECOMMENDATIONS..... | 61 |
| 7. REFERENCES..... | 65 |
| CURRICULUM VITAE..... | 71 |

ABBREVIATIONS

| | |
|--------------|--|
| ANN | : Artificial Neural Network |
| ASTER | : Advanced Spaceborne Thermal Emission and Reflection Radiometer |
| BU | : Built-Up |
| DN | : Digital Number |
| EBBI | : Enhanced Built-Up and Bareness Index |
| ER | : Electromagnetic Radiation |
| EROS | : Earth Resources Observation and Science |
| ETM | : Enhanced Thematic Mapper |
| IBI | : Index-based Built-up Index |
| MNDWI | : Modified Normalized Difference Water Index |
| MSS | : Multispectral Scanner system |
| NASA | : National Aeronautics and Space Administration |
| NDBI | : Normalized Difference Built-up Index |
| NDBaI | : Normalized Difference Bareness Index |
| NIR | : Near Infrared |
| OLI | : Operational Land Imager |
| SAVI | : Soil Adjusted Vegetation Index |
| SWIR | : Short Wave Infrared |
| TIR | : Thermal Infrared |
| TM | : Thematic Mapper |
| TOA | : Top of Atmosphere |
| UI | : Urban Index |
| USGS | : U.S. Geological Survey |

LIST OF TABLES

| | <u>Page</u> |
|--|-------------|
| Table 5.1 : Technical information of Landsat 5 TM..... | 37 |
| Table 5.2 : Characteristics of Landsat 5 TM..... | 37 |
| Table 5.3 : Technical information of Landsat 8 OLI & TIRS..... | 38 |
| Table 5.4 : Characteristics of Landsat 8 OLI & TIRS. | 38 |
| Table 5.5 : The dates of Landsat data used | 39 |
| Table 5.6 : Extracted urban indices from Landsat5 TM imagery. | 41 |
| Table 5.7 : Extracted urban indices from Landsat8 OLI & TIRS imagery..... | 42 |
| Table 5.8 : Threshold values of the index value for each type of index transformation in determining non-built-up, built-up for August 20, 2003 Landsat 5 TM Image..... | 49 |
| Table 5.9 : Threshold values of the index value for each type of index transformation in determining non-built-up, built-up for September 06, 2015 Landsat OLI & TIRS Image. | 49 |
| Table 5.10 : Impervious surface and bare land areas of each index for August 20, 2003 Landsat 5 TM Image..... | 50 |
| Table 5.11 : Impervious surface and bare land areas of each index for September 06, 2015 Landsat 8 OLI & TIRS Image. | 51 |
| Table 5.12 : Impervious surface and bare land area of farmland for each index for August 20, 2003 Landsat5 TM Image. | 56 |
| Table 5.13 : Impervious surface and bare land area of farmland for each index for September 06, 2015 Landsat8 OLI & TIRS Image. | 56 |
| Table 5.14 : Impervious surface and bare land area of farmland of each index for August 20, 2003 TM Image..... | 57 |
| Table 5.15 : Impervious surface and bare land areas of farmland of each index for September 06, 2015 Landsat8 OLI & TIRS Image. | 57 |
| Table 5.16 : Length of road of each index for August 20, 2003 Landsat5 TM Image. | 58 |
| Table 5.17 : Length of road of each index for September 06, 2015 Landsat8 OLI & TIRS Image..... | 58 |
| Table 5.18 : Accuracy assessment result table..... | 59 |

LIST OF FIGURES

| | <u>Page</u> |
|---|-------------|
| Figure 1.1 : Global distribution and density of constructed impervious (Elvidge et al, 2007) | 2 |
| Figure 2.1 : Impervious surfaces vs pervious surfaces (http://www.mdcoastalbays.org). | 6 |
| Figure 3.1 : Passive and active sensors (www.wikipedia.org)..... | 9 |
| Figure 3.2 : Electromagnetic waves (www.shariqa.com) | 10 |
| Figure 3.3 : Electromagnetic spectrum (Borges, 2008) | 11 |
| Figure 3.4 : Spectral signature of the none urban features (Ramesh et al, 1995). | 13 |
| Figure 3.5 : (a) Spectral reflectance distribution in 450-900 nm wavelength region for brick road surface; (b) Bituminous road surface; (c) Bituminous rooftop surface (Ramesh et al, 1995)..... | 14 |
| Figure 3.6 : Comparison of spectral reflectance characteristics of brick, and bituminous roads, and bituminous rooftops surfaces (Ramesh et al, 1995). | 15 |
| Figure 4.1 : Digital image. | 21 |
| Figure 4.2 : Spectral profiles of six typical land covers for Landsat8 OLI & TIRS... .. | 25 |
| Figure 4.3 : Density slicing. | 29 |
| Figure 4.4 : The error matrix (Foody, 2002)..... | 30 |
| Figure 5.1 : Location of the Istanbul..... | 35 |
| Figure 5.2 : Landsat 5 TM - 20/08/2003 data (a) Frame 180/ 31 (b) Frame 180/ 32 (c) Mosaic and subsetted image..... | 40 |
| Figure 5.3 : Flowchart of estimating impervious surface and bare land fraction in the study..... | 43 |
| Figure 5.4 : NDBI images of Istanbul (a) August 20, 2003 (b) September 06, 2015..... | 44 |
| Figure 5.5 : NDBaI images of Istanbul (a) August 20, 2003 (b) September 06, 2015 | 45 |
| Figure 5.6 : UI images of Istanbul (a) August 20, 2003 (b) September 06, 2015..... | 46 |
| Figure 5.7 : EBBI images of Istanbul (a) August 20, 2003 (b) September 06, 2015..... | 47 |
| Figure 5.8 : IBI image of Istanbul (a) August 20, 2003 (b) September 06, 2015..... | 48 |
| Figure 5.9 : Validation of EBBI index image of August 20, 2003 classified as impervious surface and bare land using Quickbird August 03, 2003 image as reference..... | 51 |
| Figure 5.10 : The spatial distribution of impervious surfaces and bare lands is shown for each type of index/remote sensing data transformation for August 20, 2003 Landsat5 TM Image: (a) EBBI, (b) IBI, (c) NDBI, (d) UI, (e) NDBaI..... | 52 |

| | |
|--|-----------|
| Figure 5.11 : The spatial distribution of impervious surfaces and bare lands is shown for each type of index/remote sensing data transformation for September 06, 2015 Landsat8 OLI & TIRS Image: (a) EBBI, (b) IBI, (c) NDBI, (d) UI, (e) NDBaI..... | 53 |
| Figure 5.12 : Missclassification of bare land as impervious surface in NDBI image Landsat5 TM August 20, 2003 in contrast to Quickbird August 03, 2003 image..... | 54 |
| Figure 5.13 : Ataturk airport land cover extraction by urban indices..... | 55 |
| Figure 5.14 : Farmland west of Istanbul (Quickbird)..... | 56 |
| Figure 5.15 : Impervious surface and bare land area of farmland of each index for August 20, 2003 TM Image..... | 57 |
| Figure 5.16 : Impervious surface and bare land areas of farmland of each index for September 06, 2015 Landsat OLI & TIRS Image..... | 57 |
| Figure 5.17 : Road by the Buyukcavuslu (WorldView-3)..... | 58 |

IMPERVIOUS SURFACE ESTIMATION AND MAPPING VIA REMOTELY SENSED TECHNIQUES

SUMMARY

Land cover and land use of earth has significantly been changed by unplanned and uncontrolled expansion of urban areas throughout time and the increasing change by the passing years, were verified by various studies. Only remote sensing from space, can provide the global, repeatable, continuous observations of processes, needed to understand the Earth system as a whole. Remote sensing data can be used in several applications such as, meteorological data collection, change detection and land cover mapping, urban planning, climate change, disaster monitoring and so on. One of the important applications of remote sensing is to detect, monitor and map impervious surfaces in urban areas. Impervious surfaces are present in many areas of the world. The areas most affected by this change are developing countries and the metropolitan cities, which are under pressures due to an unprecedented increase in population growth and developments as the result of urbanization and industrialization.

Land Use and Land Cover (LULC) and Impervious Surface Area (ISA) are important parameters for many environmental studies, and serve as an essential tool for decision makers and stakeholders in Urban & Regional planning. Istanbul is among the cities that is facing the problem of a large amount of land cover changes because of various factors specifically urbanization and population growth. Urbanization phenomena with all its advantages for people, causes the large portion of land cover and land use change in mega cities such as Istanbul. Available medium spatial resolution satellite imagery, in combination with Remote Sensing techniques, are very important sources in analyzing the urban areas. Classification of Landsat images using remote sensing indices are the mostly used and simple methodology for detecting and extracting the impervious surface and bare land classes.

In this study, the Impervious surface area and bare land determination of Istanbul from years, 2003 and 2015 were analyzed using different remote sensing indices such as UI

(Urban Index), IBI (Index Based Built Up Index), NDBI (Normalized Difference Built-Up Index), NDBal (Normalized Difference Bare Land Index) and EBBI (Enhanced Based Built Up Index). Multitemporal data were acquired from freely available LANDSAT 5 TM and LANDSAT 8 OLI & TIRS satellite in two different dates (20-August-2003, 06-September-2015).

In the introduction part of the thesis, definition of remote sensing and a brief summary of the topic are given. In the second chapter, general information about artificial surface is provided. In the third chapter, the electromagnetic spectrum, radiation and electromagnetic interaction with Earth's features, spectral reflectance and remote sensing of artificial surfaces are explained. In the fourth chapter, digital image processing is defined and indices are explained.

In the application chapter, the study area Istanbul and the data used including satellite data are defined. In this study, it is aimed to evaluate the impervious surfaces and bare lands in the study area, using remote sensing indices; and to analyze the potential of each urban index specially EBBI index since this study is among the first to apply this index on a heterogenous urban area and finally to produce the impervious surface map of Istanbul. With regard to the above objectives different built-up and bare soil indices were applied to analyze impervious surface and bare soil and threshold values for three categories as impervious surface, bare soil and others was decided by visual interpretation and then density slicing was applied for producing thematic map of Istanbul. Other category includes green areas, forest areas and water surfaces. Accuracy assessment was calculated for each of indices to determine how accurately the indices worked to solve classification problem of impervious surface and bare lands in heterogenous urban areas by implementing visual interpretation, digitizing for area and length, overall accuracy and Kappa statistics.

As the result of study, UI index has 90% overall accuracy for impervious surface, EBBI index presents 93% overall accuracy for bare land, IBI index has 84% overall accuracy for impervious surface, NDBI index has 73% overall accuracy for impervious surface and NDBal has 88% overall accuracy for bare land. EBBI index shows the highest impervious surface area of 121,421 ha and for the bare land NDBal index features highest area of 67,255 ha for Landsat 5 TM August 20, 2003 data. For Landsat 8 OLI & TIRS September 06, 2015 EBBI index shows 87% overall accuracy for impervious surface, NDBal index has 92% overall accuracy for bare land, IBI index

shows 89% overall accuracy for bare land, NDBI has 86% overall accuracy for bare land and UI has 87% overall accuracy for bare land. EBBI index presents the highest impervious surface area of 137,406 ha and NDBaI Index confirms highest bare land area of 56,508 ha.

It can be asserted that indices generated by utilizing the multispectral feature of Landsat imagery, which has the long-term archive of satellite images, can be used for determining the land cover/use changes. In addition, some recommendations for the future research and the problems which encountered during analysis are outlined.

UZAKTAN ALGILAMA TEKNİKLERİ İLE GEÇİRİMSİZ YÜZEY TAHMİNİ VE HARİTALANMASI

ÖZET

Bu çalışmada iki farklı tarihte elde edilmiş farklı spektral çözünürlükte Landsat uydu görüntülerinin “İstanbul” örneğinde; geçirimsiz alanların ve boş alanların belirlenmesinde kullanılabilirlikleri için uygulanabilecek farklı uzaktan algılama indeksleri ele alınmıştır. Kullanılan yöntemler ile elde edilen yeni işlenmiş görüntülerin performanslarının karşılaştırılması ile İstanbul için kullanılan indeksler arasından en doğru sonuç veren indeksin belirlenmesi hedeflenmiştir.

Gerek ülkemizde gerek dünyamızda, şehir alanların yönetilmesi ve geliştirilmesi için doğru ve güvenilir verilere ve veri elde etme yöntemlerine gereksinim duyulmaktadır. Veri desteği ile çok amaçlı haritaların üretilmesi ve bu alanların sürekli izlenmesini sağlayacak teknolojilerin kullanımı gerekmektedir. Uzaktan algılama teknolojisi farklı ölçekte, tekrarlı ve devamlı gözlemler ile yeryüzünü anlamak için kullanılan etkin bir yöntemdir. Farklı çözünürlüklere sahip uzaktan algılanmış görüntüler meteorolojik veri toplama, arazi örtüsü ve kullanımı haritalarının üretilmesi ve değişim tespiti, şehir planlama, iklim değişimi, doğal afetlerin izlenmesi gibi çok sayıda uygulamada etkin ve yaygın olarak kullanılmaktadır. Şehir alanlarında geçirimsiz yüzeylerin (yapay yüzeylerin) belirlenmesi, izlenmesi ve değişimlerinin tespit edilmesi uzaktan algılama teknolojisinin önemli uygulama alanları arasında bulunmaktadır. Geçirimsiz yüzeyler şehir alanlarının büyük bir bölümünü kaplamaktadır. Geçirimsiz yüzeyler ve bunların olumsuz etkileri en yaygın olarak şehirleşme ve endüstrileşme ve bunlara bağlı olarak gözlemlenen hızlı nüfus artışlarının meydana geldiği gelişmekte olan mega şehirlerde gözlenmektedir. Şehir alanlarının plansız ve kontrolsüz büyümesinden dolayı son yıllarda meydana gelen arazi kullanımı ve arazi örtüsü değişimleri ve bunların çevresel faktörler üzerindeki etkileri çok sayıda bilimsel çalışmada incelenmiştir.

Arazi kullanımı /örtüsü ve geçirimsiz yüzeyler çevresel çalışmalar ve bunların sonuçlarını kullanan karar vericiler için önemli parametrelerdir. Orta çözünürlükte

uydu görüntüleri ve uzaktan algıma teknikleri şehir alanlarının analizi ve sürdürülebilir yönetimi için çok önemli kaynaklardır. Uzaktan algılama indeksleri ile uydu görüntülerinin sınıflandırılması geçirimsiz yüzeylerin ve boş alanların tespit edilmesi ve izlenmesi için yaygın olarak kullanılan etkili bir yöntem olarak kabul edilmektedir.

Bu araştırmada, özellikle 1980 yılı sonrasında hızlı nüfus artışı, sanayileşme ve buna bağlı olarak yerleşim alan artışı ve farklı arazi örtüsü değişimlerinin gözlemlendiği İstanbul ili çalışma bölgesi olarak seçilmiştir. Bu tez çalışmasında, İstanbul iline ait geçirimsiz alanların ve boş alanların tespiti için farklı spektral özelliklere sahip uzaktan algılama verilerinin performanslarını analiz etmek amacı ile ücretsiz olarak elde edilebilen orta mekansal çözünürlüğe sahip Landsat 5 TM ve Landsat 8 OLI&TIRS görüntüleri kullanılmıştır.

Uygulamanın ilk aşamasında, orta mekansal çözünürlüğe sahip 20 Ağustos 2003 tarihli Landsat 5 TM ve 6 Eylül 2015 tarihli Landsat 8 OLI& TIRS görüntüleri elde edilmiştir.

Bu çalışmada, literatürde yaygın olarak kullanılan farklı uzaktan algılama indeksleri ile İstanbul geçirimsiz alanlarının ve boş alanların belirlenmesi ve farklı indekslerin performanslarının karşılaştırılması amaçlanmıştır. Çalışma kapsamında kullanılan uzaktan algılama indeksleri UI (Urban Index (Şehir İndeksi)), IBI (Index Based Built Up Index (İndeks tabanlı yapay alan indeksi)), NDBI (Normalized Difference Built-Up Index (Normalleştirilmiş Fark Yapay Alan İndeksi)), NDBal (Normalized Difference Bare Land Index (Normalleştirilmiş Fark Boş Alan İndeksi)) ve EBBI (Enhanced Based Built Up Index (Zenginleştirilmiş Yapay Alan ve Boş Alan İndeksi)) olarak belirlenmiştir. İndekslerin tümü Landsat 5 TM ve Landsat 8 OLI & TIRS görüntülerinin ilgili bantları kullanılarak hesaplanmıştır. Özellikle seçilen indeksler arasında ıslık bant kullanılan tek indeks olan EBBI indeksi bu çalışma ile ilk defa heterojen özelliklere sahip bir mega şehir alanında kullanılmıştır. Ayrıca görüntü bantları kullanılarak hesaplanan farklı indekslerin kullanılması ile hesaplanan tek indeks olma özelliği taşıyan IBI indeksi bu çalışmada hem Landsat 5 TM hem de yeni nesil Landsat 8 OLI & TIRS görüntüsüne uygulanmıştır. Her indeks için görsel yorumlama yöntemi ile eşik değerler üç farklı sınıf için (geçirimsiz yüzeyler, boş alanlar ve diğer) belirlenmiştir. Belirlenen eşik değerler kullanılarak yoğunluk dilimleme yöntemi ile İstanbul için tematik haritalar oluşturulmuştur. Farklı indekslere ait performansların karşılaştırılması için doğruluk değerlendirmesi görsel yorumlama,

alan ve uzunluk hesaplamaları için sayısallaştırma, genel doğruluk ve Kappa istatistiği hesaplamaları ile gerçekleştirilmiştir. İstanbul için Landsat 5 TM ve Landsat 8 OLI &TIRS görüntüleri ile geçirimsiz yüzeylerin ve boş alanların doğru ve güvenilir olarak belirlenebildiği indeksler belirlenmiştir. . Sonuç olarak, Landsat 5 TM (20 Ağustos 2003) görüntüsü ile en yüksek genel doğruluk EBBI indeksi kullanılarak elde edilmiştir. 2003 tarihli görüntü ile hesaplanan indeksler için genel doğruluk değerleri geçirimsiz yüzeyler ve boş alanlar için karşılaştırıldığında EBBI indeksi kullanılarak yüksek genel doğruluk boş alan için % 93, IBI indeksi kullanılarak yüksek genel doğruluk geçirimsiz yüzeyler için % 84, NDBI indeksi kullanılarak yüksek genel doğruluk geçirimsiz yüzey için % 73, UI indeksi ile yüksek genel doğruluk geçirimsiz yüzeyler için % 90 ve NDBal indeksi ile yüksek genel doğruluk boş alan için % 88 olarak hesaplanmıştır. Landsat 8 OLI & TIRS (06 Eylül 2015) görüntüsü ile en yüksek genel doğruluk NDBal indeksi kullanılarak % 90.3 olarak edilmiştir. 2015 tarihli görüntü ile hesaplanan indeksler için genel doğruluk değerleri geçirimsiz yüzeyler ve boş alanlar için karşılaştırıldığında EBBI indeksi kullanılarak yüksek genel doğruluk geçirimsiz alanlar için % 87, IBI indeksi kullanılarak yüksek genel doğruluk boş alan için % 89, NDBI indeksi kullanılarak yüksek genel doğruluk boş alan için % 86, UI indeksi ile yüksek genel doğruluk boş alan için % 87 ve NDBal indeksi ile yüksek genel doğruluk boş alan için % 92 olarak hesaplanmıştır. Bu çalışma ile uzaktan algılama indeksleri uzun ve sürekli zaman arşivine sahip orta çözünürlüklü çok bantlı Landsat görüntüleri ile heterojen bir yapıya sahip İstanbul için kabul edilebilir doğrulukta geçirimsiz yüzeylerin ve boş alanların belirlenmesinde etkin olarak kullanılabilceğini gösteren bir altlık çalışma gerçekleştirilmiştir.

1. INTRODUCTION

Land-Use and Land Cover (LULC) changes are among the most important factors for environmental change such as deforestation, urbanization, climate change and natural disaster management (Turner II et al, 1995). Urban areas have been expanding very fast and rates of population growth in urban areas are higher than the overall population growth in most countries. This happens because urban areas are the focus of economic activities and transportation hubs (Masek et al, 2000). Urban land changes, referred to as urban sprawl, have effects for the environmental and socio- economic sustainability of communities (Xu, 2007). Accurate LULC maps are needed for urban planning and natural resource issues like open space preservation, forest management, urban growth and losses of farm or natural lands, these maps have to distinguish accurately features of the built environment from vegetation in the area.

Impervious surfaces are anthropogenic features through which water cannot infiltrate into the soil, such as roads, driveways, sidewalks, parking lots, rooftops, and so on. In recent years, impervious surface has emerged not only as an indicator of the degree of urbanization, but also a major indicator of environmental quality (Arnold and Gibbons, 1996). The total ISA of the world is estimated to be 579,703 km². This is nearly the same size as the country of Kenya (584,659 km²). The country with the most ISA is China (87,182 km²) followed closely by the United States (83,881 km²), and India (81,221 km²) (Elvidge et al, 2007) (Figure 1.1).

A requirement for the quantitative study of environmental issues caused by the increasing impervious surface is to obtain detailed information of impervious surface in an urban area. Knowledge on impervious surfaces, especially the magnitude, location, geometry, spatial patterns and the perviousness-imperviousness ratio, is significant to a range of issues and themes in environmental science (Weng, 2012). Therefore, accurate impervious surface mapping in the urban areas has recently attracted unprecedented attention from natural scientists throughout the world (Weng, 2012).

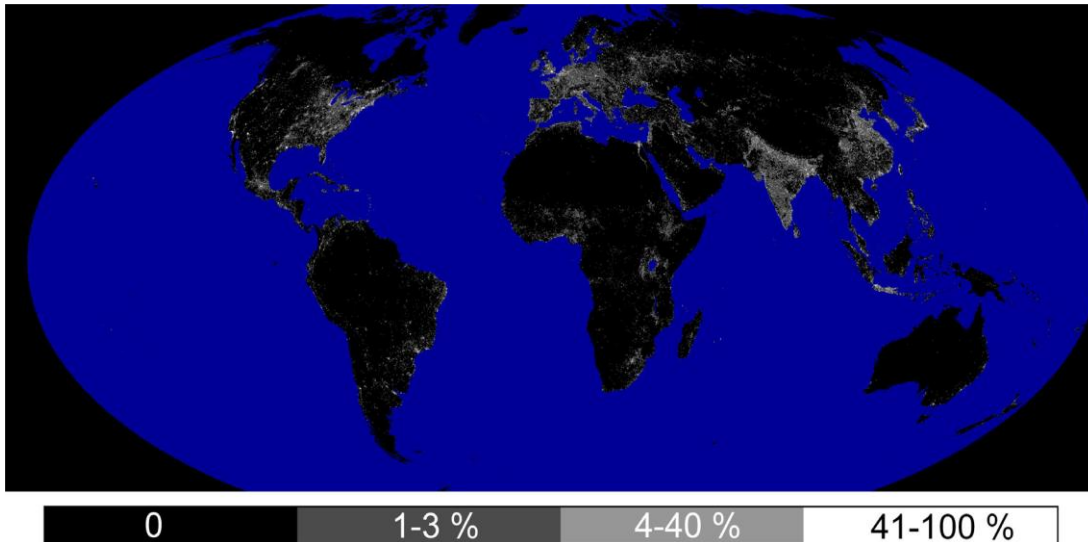


Figure 1.1: Global distribution and density of constructed impervious (Elvidge et al, 2007)

Istanbul as Turkey's largest city and also biggest city in Europe by population within city limits, has always been under pressure of rapid urbanization because of its superiority in historic, culture and specifically for its economic opportunities (Balik Sanli et al, 2008). Urbanization development and population growth resulted in drastic changes in the land cover of Istanbul through centuries. Istanbul has been always confronted the illegal housing problem (Keyder, 2005). Beside this moot point, planned urbanization itself means the change in the land cover and somehow damages to the nature of Istanbul. It is obvious that there is no stopping for urbanization operation and land cover change that has resulted because of that, so the land managers and people liable for the consequences of changes in land cover of the city should develop new methods and practical techniques for decreasing negative effects caused by urbanization as much as possible (Mundhe and Jaybhaye, 2014). Vegetation cover decreasing and its after effects, problems related to climate change, increasing of impervious lands are some of adverse impacts of urbanization and land cover change processes (Jiang et al, 2015). For monitoring spatial changes that occurred through years and planning to solve problems of land cover changes, the trend of change in previous years should be studied and the future planning should be done by considering this trend of change (Bellard et al, 2014). Today remotely sensed data by satellites are among the most used data for such kind of studies (Song et al, 2014). Image data files of freely available medium spatial resolution data of Landsat products are reliable data for detecting and studying changes through years.

Mapping the impervious surfaces in urban areas is important because the existence of these types of land can be used as an indicator of urban development and environmental quality. The mapping process applies different remotely sensed data and spectral values based on the land use category. Urban change detection in Istanbul has been investigated by researchers previously ((Musaoglu et al, 2006), (Kaya and Curran, 2006), (Balik Sanli et al, 2008), (Geymen and Baz, 2008)). For detecting the changes, there are some methods. Classification is the method which was used by Van Niel, (1995), Yuan et al. (2005), Coban et al. (2010) through the application of multi temporal images of the specific area. In this method, the classes are separated and the size of each class is determined. Another method is using the bare soil and built-up indices which are graphical indicators used to detect the target such as impervious surface and its magnitude and intensity. Chen et al. (2006) classified urban land uses using several remote sensing indices in the Pearl River Delta of China with high accuracy. Indices for mapping impervious surfaces in urban areas, such as the Urban Index (UI) Kawamura et al. (1996), Bare soil index (BI) Rikimaru and Miyatake (1997), Normalised Difference Built-Up Index (NDBI) Zha et al. (2003), Normalised Difference Bareness Index (NDBaI) Zhao and Chen (2005), Index-based Built-Up Index (IBI) Xu (2008), and Enhanced Built-Up and Bareness Index (EBBI) As-syakur et al. (2012) have been employed in various studies.

The main objectives of this study are: (1) to understand the spectral reflectance characteristics of impervious surfaces of Istanbul, (2) to explore the potential of Landsat 5 TM and Landsat 8 OLI & TIRS imagery to detect and map the impervious surface over the study area.

In the framework of this study, impervious Surface and bare land detection is being analyzed using freely available Landsat 5 TM and Landsat 8 OLI & OLI data (2003, 2015) in Istanbul, Turkey. Several built-up, bare soil indices were examined and maps were produced. Finally accuracy assessment showing the precision of this study was examined.

2. ARTIFICIAL SURFACE

2.1 Artificial Surfaces Defined and Described

The phrase artificial surfaces or “impervious surfaces” is a relatively new and descriptive expression used to characterize certain land cover types found in urban areas. The term impervious generally refers to something that is impenetrable or that does not allow entrance or passage through (Merriam Webster, 1994). Impervious surfaces are anthropogenic features through which water cannot infiltrate into the soil, such as roads, driveways, sidewalks, parking lots, rooftops, and so on. In recent years, impervious surface has emerged not only as an indicator of the degree of urbanization, but also a major indicator of environmental quality (Arnold and Gibbons, 1996). As a result, surfaces that do not allow the penetration or passage of another substance can be considered impervious surfaces. Specific to this research, impervious surfaces will be defined as any surface that does not allow the natural infiltration of water.

In any urban area, many different land cover types constitute impervious surfaces, such as paved roads, sidewalks, driveways, parking lots and rooftops. They are typically land cover types constructed from impervious materials such as asphalt, concrete, brick and stone. When these materials are applied to an area, they create an effective seal against the infiltration of water resulting in impervious surfaces.

Generally, most of the impervious surface land cover types found in urban areas can be categorized as belonging to either transportation (roads, sidewalks, driveways, parking lots, etc.), or rooftop (residential housing, buildings, etc.). From these two major categories, those attributed to transportation are typically the largest contributors to total impervious area (Schueler, 1994) (Figure 2.1).

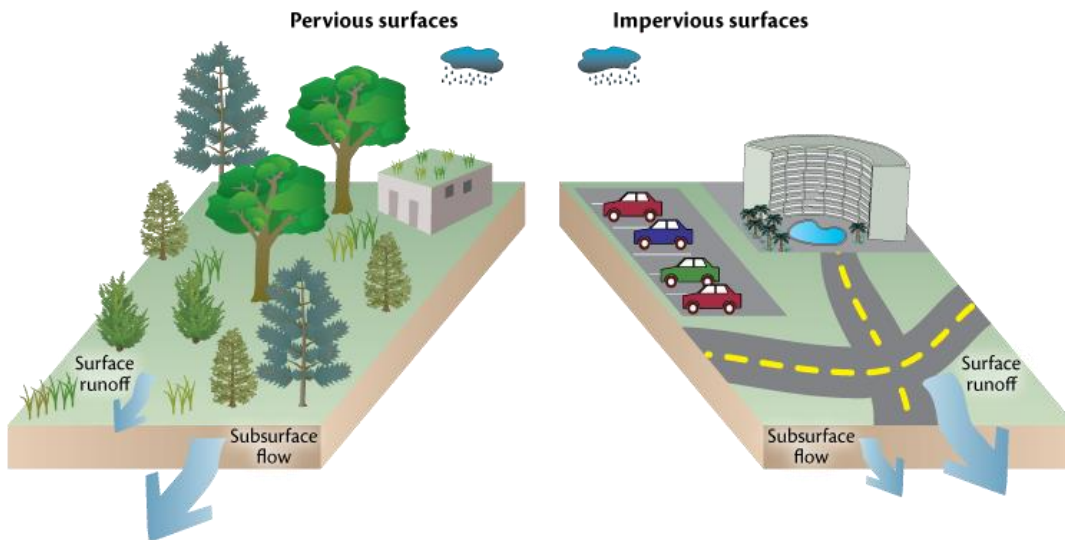


Figure 2.1 : Impervious surfaces vs pervious surfaces
 (<http://www.mdcoastalbays.org>).

2.2 Development of Impervious Surfaces as an Environmental Indicator

Impervious surfaces have become an important variable for determining the overall environmental health of a watershed. The extent of their presence tends to have a profound effect upon the natural processes that normally occur within watersheds. The most obvious of these effects is the increase in volume of surface runoff during storm events. As more and more of a watershed's area are covered with impervious surfaces, the volume of surface runoff from that watershed also increases. This occurs primarily because covering an area with impervious material tends to make it more hydrologically active, meaning the area is sealed from infiltration and thereby generates surface runoff. A study by Novotny and Chesters (1981) indicated surfaces created from impervious materials such as asphalt or concrete, the predominant impervious material in urban areas, are nearly 100 percent hydrologically active.

The magnitude, location, geometry and spatial pattern of impervious surfaces, and the pervious–impervious ratio in a watershed have hydrological impacts. Although land use zoning emphasizes roof related impervious surfaces, transport-related impervious surfaces could have a greater impact. The increase of impervious cover would lead to the increase in the volume, duration, and intensity of urban runoff (Weng, 2012). Watersheds with large amounts of impervious cover may experience an overall decrease of groundwater recharge and baseflow and an increase of stormflow and flood frequency (Brun and Band, 2000). Furthermore, imperviousness is related to the water

quality of a drainage basin and its receiving streams, lakes, and ponds. Increase in impervious cover and runoff directly impact the transport of non-point source pollutants including pathogens, nutrients, toxic contaminants, and sediment (Hurd and Civco, 2004).

As discussed earlier, the definition and description of impervious surfaces for this research was one that does not allow for the infiltration of water and can primarily be categorized as belonging to either a transportation or rooftop land cover type. Additionally, they are mainly a constructed surface that represents the imprint of land development on the landscape. As the process of land development begins, impervious surfaces are added in the forms of homes and driveways, shopping centers and parking lots, streets and highways. Eventually, as various forms of impervious surfaces are added, rural landscapes are replaced with urban communities. In effect, impervious surfaces are a cultural by product of how urban communities are organized, stimulated and protected. Because of the significant increases in impervious surfaces and urbanization that has occurred during the last 50 years, it is intuitively rational that many investigators such as Arnold and Gibbons (1996), Schueler (1994) and Sleavin et al. (2000) refer to urban development as being synonymous with increases in impervious surfaces.

Although increases in impervious surfaces can be correlated with increases in urbanization, it is conceptually more important to recognize that impervious surfaces are the common variable to many of the aforementioned effects on environmental processes. This has led Schueler (1994) to advocate the use of impervious surfaces as a unifying theme to help assess, mitigate and manage aquatic ecosystems. Similarly, Arnold and Gibbons (1996) describe impervious surfaces as a valuable tool for both protecting and managing water resources. In areas where few records or little detailed information is available, they hypothesize impervious surfaces might be the most cost effective and feasible parameter for addressing issues related to water resources. They attribute this value to two major factors, the first of which is impervious surfaces are integrative. This means a more uniform and consistent analysis can be reached about water resources because inherent complexities associated with specific environmental processes can be avoided.

The second factor is impervious surfaces are measurable (Arnold and Gibbons 1996). This means its physical size or area can be determined and short of being modified or

destroyed, its results, once measured, are reproducible. Therefore, depending on the size of the area considered and purpose for which it is to be applied, a wide range of techniques exists for the measuring of impervious surfaces.

3. REMOTE SENSING OF ARTIFICIAL SURFACES

3.1 Principles of Remote Sensing

Remote sensing is the science of obtaining information about objects from a distance and not being in contact with the object of interest. Information is gathered by the processes of recording, measuring and interpreting of the imagery, derived typically from aircrafts or satellites (Jensen, 2009).

Remote sensors can be either passive or active (Figure 3.1). Passive sensors record radiation that is reflected from Earth's surface, where the sun plays the role of providing an energy source and illuminates the target. Because of this, passive sensors can only be used to collect data during daylight hours; however, active sensors emit signals to the Earth's surface and record the backscattered or reflected signals.

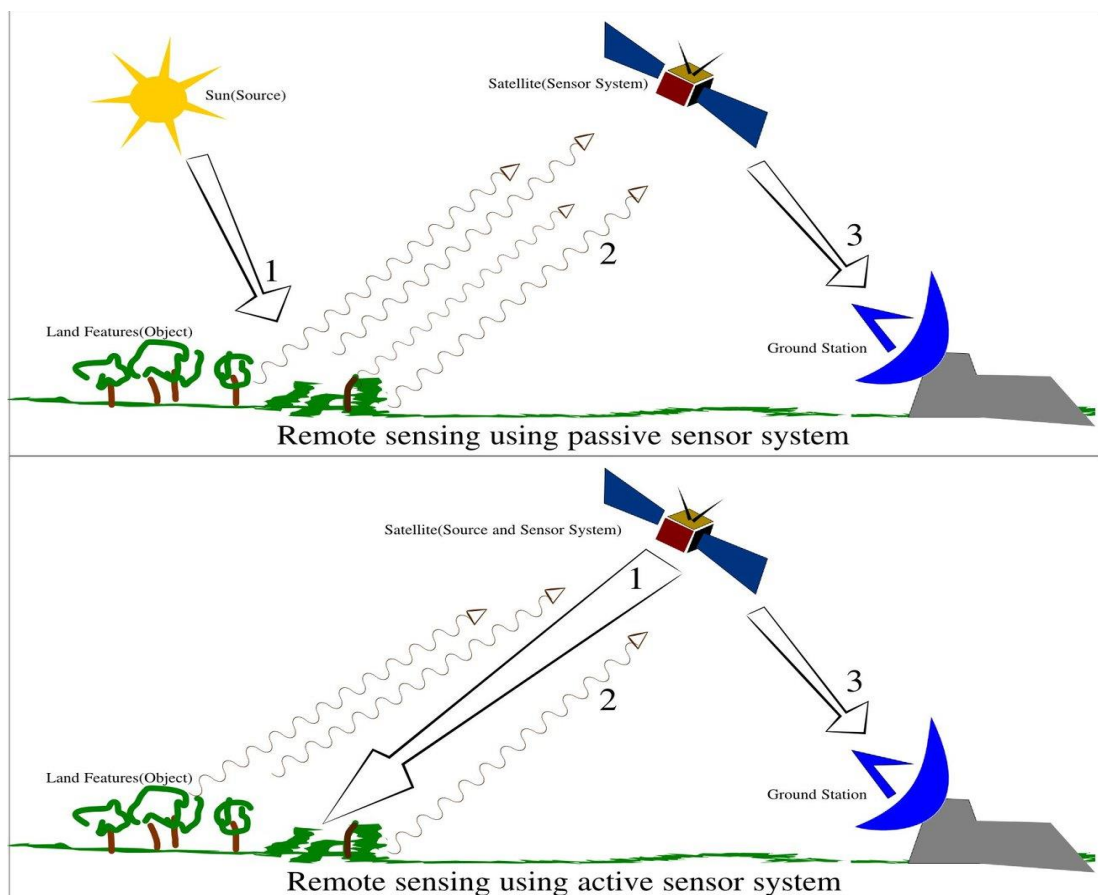


Figure 3.1 : Passive and active sensors (www.wikipedia.org)

The radiation from the sun or satellite system incident upon the Earth's surface causes three different interactions with objects: It can be absorbed, transmitted or reflected. The reflected energy is the most useful one in remote sensing applications. Reflection occurs when a ray of light is redirected as it strikes a non-transparent surface. Transmission of radiation occurs when radiation passes through a substance without significant attenuation. Absorption occurs when all the electromagnetic radiation is absorbed by objects on the Earth's surface and converted into the other form of energy or reradiated at a larger wavelength (Joseph, 2005) .

3.2 Electromagnetic Spectrum and Radiation

Electromagnetic wave's energy transports energy through space in the form of periodic disturbances of electric and magnetic fields (Figure 3.2). All electromagnetic waves travel through space at the same speed, $c=2.99792458 \times 10^8$ m/s, commonly known as the speed of light. An electromagnetic wave is characterized by a frequency and wavelength.

These two quantities are related to the speed of light by the equation:

$$\text{Speed of light} = \text{frequency} \times \text{wavelength} \quad (3.1)$$

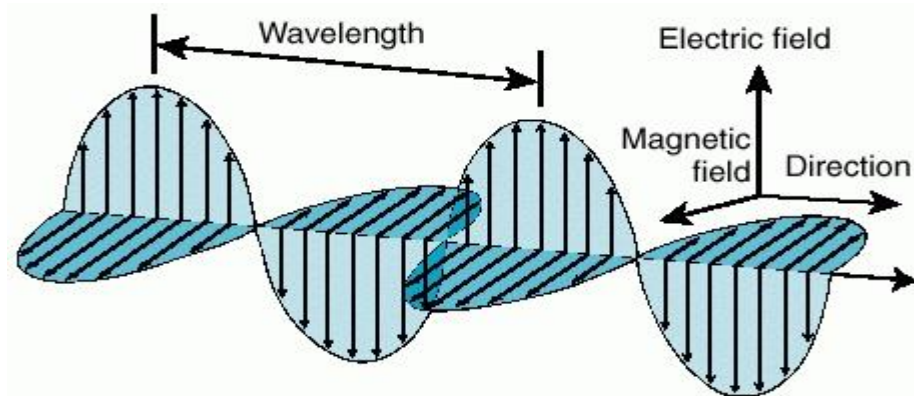


Figure 3.2 : Electromagnetic waves (www.shariqa.com)

Light is a particular type of electromagnetic radiation that can be seen and sensed by the human eye, but this energy exists at a wide range of wavelengths. The micron is the basic unit for measuring the wavelength of electromagnetic waves. The spectrum of waves is divided into sections based on wavelength (Figure 3.3). The shortest waves are gamma rays, which have wavelengths of $10e-6$ microns or less. The longest waves are radio waves, which have wavelengths of many kilometres. The range of visible

region consists of the narrow portion of the spectrum, from 0.4 microns (blue) to 0.7 microns (red) (Campbell, 1996).

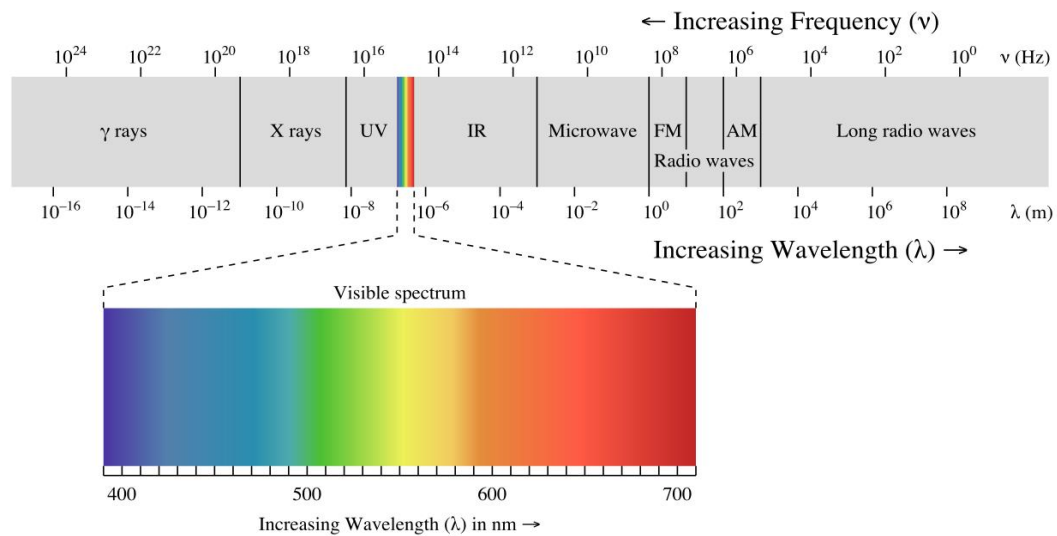


Figure 3.3 : Electromagnetic spectrum (Borges, 2008)

Electromagnetic radiation is reflected or absorbed mainly by several gases in the Earth’s atmosphere; among the most important ones are water, carbon dioxide and ozone. Some radiation, such as visible light, largely passes (transmitted) through the atmosphere. These regions of the spectrum with wavelengths that can pass through atmosphere are referred to as “atmospheric window “. Some microwaves can even pass through clouds, which make them the best wavelength for transmitting satellite communication signals (Elachi and Van Zyl, 2006).

Electromagnetic radiation could be redirected due to the presence of particles and gasses in the atmosphere; in this case, three different scattering mechanisms can occur:

Rayleigh scattering: It happens when the wavelength of the radiation is smaller than the particles in atmosphere such as dust and oxygen molecules.

Mie scattering: It happens when the particles in the atmosphere are almost the same size as the wavelength of radiation. Smoke, dust and water vapour are the common cause of Mie scattering.

Nonselective scattering: It happens when particles are larger than the wavelength of radiation; in this case, all wavelengths scatter almost equally. Water droplets and large dust particles can cause this type of scattering.

3.3 Electromagnetic Interaction with Earth's Features Spectral Reflectance

Objects having different surface features reflect or absorb the sun's radiation in different ways. The reflectance properties of an object depend on the particular material, its physical and chemical state (e.g. moisture) and the surface roughness as well as the geometric circumstances (e.g. incidence angle of the sunlight). The most important surface features are colour, structure and surface texture.

The amount of energy reflected from the surfaces is usually expressed as a percentage of the amount of energy striking the objects. Reflectance is 100% if all of the light striking an object bounces off and is detected by the sensor. If none of the light returns from the surface, reflectance is said to be 0%. In most cases, the reflectance value of each object for each area of the electromagnetic spectrum is somewhere between these two extremes.

Across any range of wavelengths, the percent reflectance values for landscape features such as water, sand, roads, forests, etc. can be plotted and compared. Such plots are called "spectral response curves" or "spectral signatures". Differences among spectral signatures are used to help classify remotely sensed images into classes of landscape features since the spectral signatures of like features have similar shapes. The figure below shows differences in the spectral response curves for main features (Figure 3.4).

Spectral information, recorded by a sensor can be extracted from the spectral signatures. Hyperspectral sensors have much more detailed signatures than multispectral sensors, and thus provide the ability to detect more subtle differences in aquatic and terrestrial features (Curran, 1985).

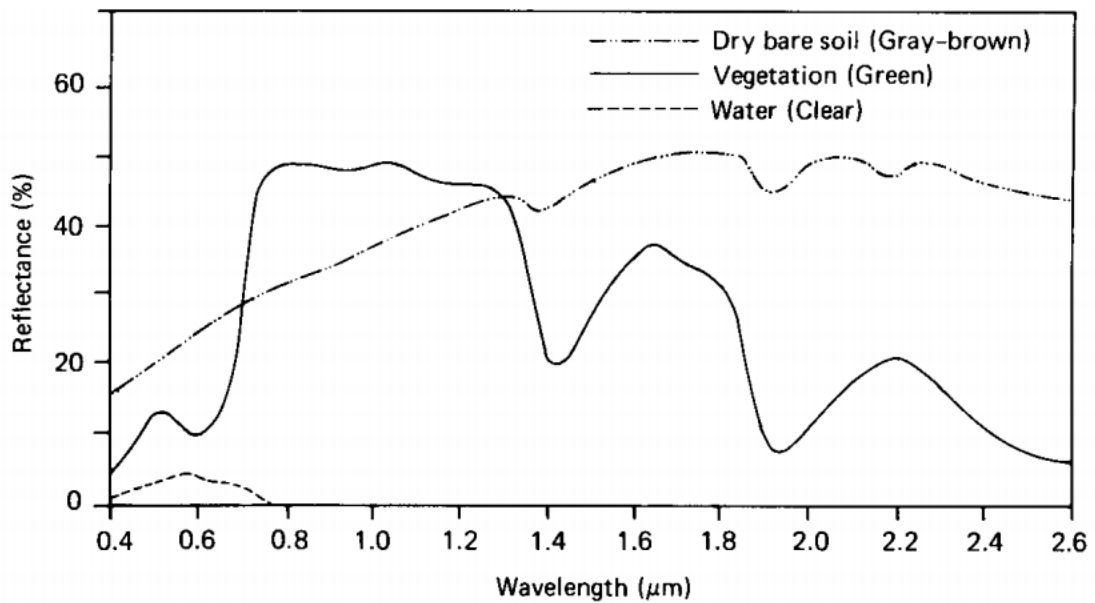


Figure 3.4 : Spectral signature of the none urban features (Ramesh et al, 1995).

3.3.1 Built up reflectance

In urban areas, impervious surfaces are made up of different kinds of materials. The maintenance of these surfaces, especially in metropolitan cities, is difficult. Now, with advancements in digital remote sensing data analysis techniques and with the availability of high resolution imagery, the assessment and evaluation of the status of these surfaces can be done on a routine basis. Remote sensing can be very useful in urban planning and management. This is only possible if we have a-priori information about the spectral signature of these surfaces. Urban area reflectance is a function of material properties of various types of impervious surfaces such as brick, mud, and bituminous roads and bituminous rooftops (Ramesh et al, 1995).

Brick Road: The brick road consists of man-made light red c1in-baked bricks. Figure. 3.5a presents the spectral reflectance curve for the brick road surface. This figure shows the direct relationship of reflectance to wavelength in the spectral region; i.e., the reflectance continuously increases with the wavelength. The obtained data points are depicted by error bars (standard error from the mean) and the spectral reflectance curve is drawn as the best fit curve for these data points. The value of spectral reflectance is minimum (0.28) at the 485 nm wavelength and maximum (0.50) around the 850 nm wavelength range (Ramesh et al, 1995).

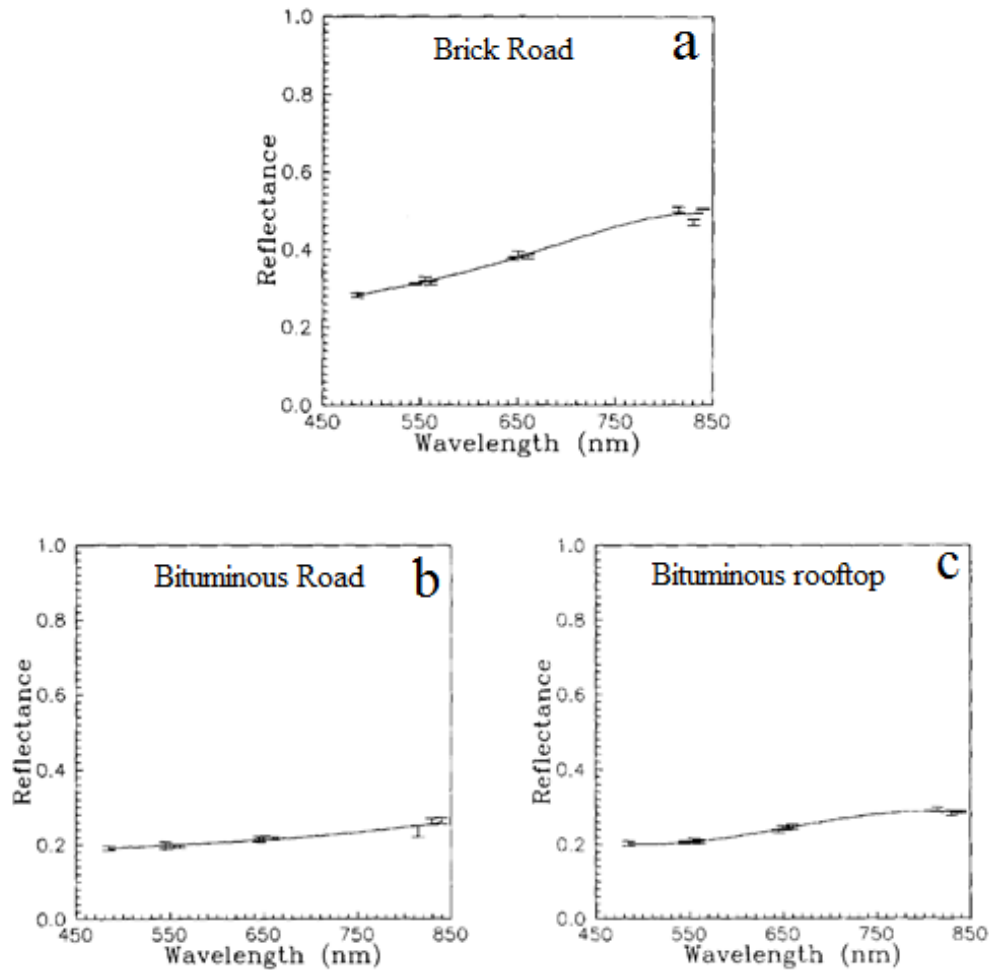


Figure 3.5 : (a) Spectral reflectance distribution in 450-900 nm wavelength region for brick road surface; (b) Bituminous road surface; (c) Bituminous rooftop surface (Ramesh et al, 1995).

Bituminous Road: This surface is a very dark brownish-black color. Fig. 3.5(b) shows the spectral reflectance properties for this surface. The data points are shown by error bars (standard error from the mean) and the curve is drawn as the best fit for these data points. This figure shows the direct relationship between reflectance and wavelength. The reflectance shows a very small variation with the wavelength in the considered wavelength range, with minimum value (0.18) at the 485 nm wavelength and maximum value (0.25) around the 850 nm wavelength. In the visible range (450-700 nm), the reflectance is low because of the very dark coloured surface. In the near infrared range (700-850 nm), the reflectance is low (but relatively higher than that in the visible range). This may be due to the surface's roughness (as absorbance is more for rough surfaces) and its other complex parameters (Fig. 3.5(b)).

Bituminous Rooftops: This is a dark reddish-brown surface and is relatively lighter in color than the bituminous road. The composition and proportion of the construction material used in the rooftop is different from that of the road and, hence, the difference in color. Fig. 3.5(c) shows the spectral reflectance characteristics of the bituminous rooftop. The data points are shown by the error bars (standard error from the mean) and the spectral reflectance curve is drawn as the best fit curve for the obtained data points. The reflectance is directly related to the wavelength in the considered wavelength range. In this case, the reflectance shows small variation with the wavelength but the variation is certainly more than that of the bituminous road. The minimum reflectance (0.20) is observed at the 485 nm central wavelength and the maximum reflectance (0.32) is observed around the 850 nm central wavelength. The low reflectance in the visible region is because of the dark colored surface. The relatively higher reflectance in the near-infrared region may be attributed to surface roughness, type of construction material, and other complex parameters. The low reflectance in the visible region is because of the dark colored surface.

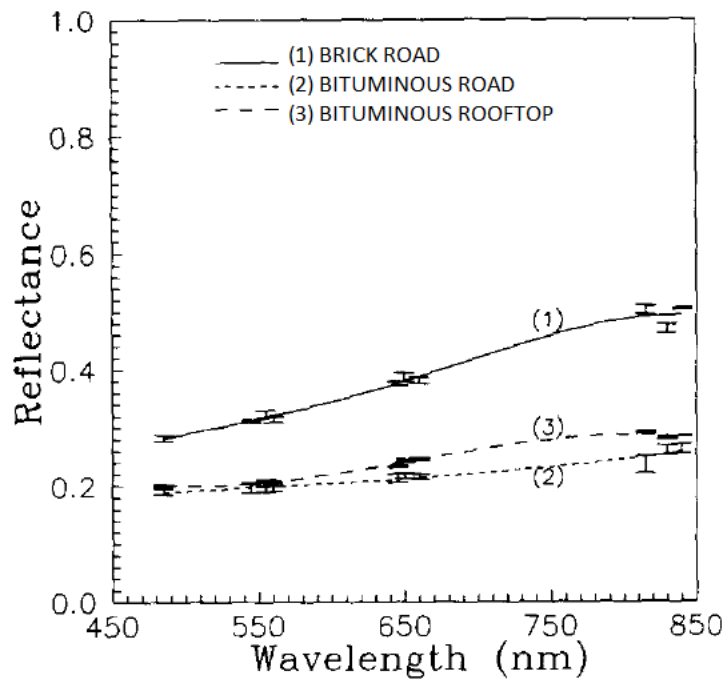


Figure 3.6 : Comparison of spectral reflectance characteristics of brick, and bituminous roads, and bituminous rooftop surfaces (Ramesh et al, 1995).

Figure 3.6 shows the spectral reflectance curves for brick, bituminous roads, and bituminous rooftop surfaces. These surfaces possess reflectance profiles typical of man-made materials; i.e., generally increasing reflectance with increasing wavelength.

The reflectance curves of these surfaces are similarly shaped, and differ only in their relative positions. The properties of brick road surface show contrast with those of the bituminous road and rooftop surfaces and can be easily distinguished from the other two surfaces in the entire wavelength range. Brick road surfaces also present contrasting properties in the entire wavelength range and can be very easily distinguished from each other. The reflectance pattern for the bituminous road and rooftop is less distinctive, but these two can be differentiated from each other in the red region of the visible spectrum (around the 650 nm wavelength).

Brick road surfaces possess a higher reflectance than those of the other two bituminous surfaces, both in the visible and near-infrared regions of the spectrum. The brick road has higher reflectance values than the other two bituminous surfaces because of its brick-red color, which is relatively lighter than the dark brownish-black of the bituminous road and dark reddish-brown of the rooftops. In the near-infrared region, brick road surfaces show a relatively higher reflectance because of their color, compositional differences and so on.

The bituminous road has a relatively lower spectral reflectance than that of the rooftop, throughout the considered wavelength range, because of differences in color, composition of the construction material, and surface roughness, and other complex differences between the bituminous road and the airstrip. The bituminous road is relatively darker than the rooftop.

3.4 Techniques for Mapping and Estimating Impervious Surfaces

A discussion of the wide range of techniques used to map and estimate impervious surfaces will be presented in this section. Throughout the discussion, individual techniques will be identified and described along with any specific advantages or disadvantages associated with the technique for determining impervious surfaces. The phrase “measurement of impervious surfaces” can be appropriately applied only in the first technique described; the remaining techniques use methodical estimation. This is primarily due to the aerial extents and amounts of impervious surfaces in many of the studies. As study area size and amounts of impervious surfaces increase, it becomes more difficult to perform a direct and quantifiable measurement.

3.4.1 Optical surveying and global positioning systems

The first method involves the physical measurement and quantification of area for all impervious surfaces by either a traditional optical ground-based survey technique or through the use of a global positioning system (GPS). According to Sleavin (1999), optical surveying and GPS are the most accurate techniques; however, both require extensive fieldwork and considerable man-hours to record geographic locations for all roads, buildings, parking lots, sidewalks, etc. As a result most investigators consider these techniques prohibitively cost effective, especially when measuring impervious surfaces in large study areas.

3.4.2 Photographic interpretation

Photo interpretation uses aerial photography for estimating impervious surfaces. Draper and Rao (1986), Harris and Rantz (1964), and Saurer et al. (1983) used photo interpretation in their respective studies and considered it to be one of the most accurate methods for determining impervious surfaces estimates. However, similar to optical surveying and GPS, photographic interpretation can be time consuming and very expensive. These issues are evident in the cost and operation of sophisticated equipment such as aircraft and navigational instruments along with the skill level of experienced individuals needed to use such equipment. This is why Sleavin (1999) suggests that determining impervious surfaces from aerial photography is only practical for small study areas (i.e., town-level or sub-regional watershed).

3.4.3 Detailed maps

Estimating impervious surfaces employs the use of detailed maps. Investigators such as Martens (1968), Southard (1987), and Spencer and Alexander (1978) have all attempted to extract impervious surfaces estimations from detailed maps by overlaying them with grid frames from which to identify and quantify impervious surfaces. However, because maps are mere representations or models of reality, the identification and estimation of impervious surfaces is limited to the types of information and level of detail the maps display. This level of detail, generally referred to as scale, can be defined as the proportional distance between what is represented on the map versus what is reality (Avery and Berlin, 1992). A small-scale map covers a large geographic area with less detail as compared to a large-scale map covering a smaller geographic area with more detail. As a result, the ability to extract accurate

impervious surfaces estimates from detailed maps is a process that is highly dependent on the information represented and the scale.

3.4.4 Population density

A more indirect approach of estimating impervious surfaces is in using population densities. Stankowski (1972) developed a quantitative index of urban land use characteristics that could then be applied to water resource analyses. From his results, Stankowski suggested population density was the only independent variable needed to empirically estimate proportions of impervious surfaces associated with different degrees of urban development. He developed and used correlation values between population density and the proportions of land use in each of six urban land use categories. From those values, he weighted his land use categories by the average percentage of impervious surfaces found in each land use category. Using these weighted correlation values the amount of impervious surfaces from a particular study area could then be estimated. Although somewhat limited by inherent averaging processes, this approach was offered as a rapid and inexpensive technique for generating qualitative indices about urbanization and impervious surfaces.

3.4.5 Image classification

A fifth method for estimating impervious surfaces is the classification of remotely sensed satellite data. The general process entails the collection of reflected electromagnetic radiation from the earth's surface to sensors onboard a satellite. Depending upon the satellite, there are differences in the number of bands, individual bandwidths, and spatial resolutions that sensors onboard various satellites are able to detect and collect. Once the satellite data is collected it can be processed, formatted and geo-rectified for analysis in a digital environment. Image classification operations can then be performed.

Conceptually, the objective of digital image classification is to replace a subjective, visual analysis process with a more objective, quantitative technique for automating the identification of features in a scene. This procedure normally involves the analysis of multispectral image data and the application of statistically based decision rules for determining the feature identity of each pixel in an image. Ultimately, it is the intent of the image classification process to categorize all pixels in a digital image into one of several land use/land cover classes or "themes" (Lillesand et al, 2014).

As an early investigation into the potential of image classification, Toll (1984) evaluated Landsat MSS and TM data for discriminating between different land cover types. He noted higher levels of accuracy were achieved using Landsat TM data than the older Landsat MSS data for classifying certain urban land cover types. Prior to his investigation, there had been very few studies conducted that used remotely sensed satellite data to classify urban land cover types. The lack of interest for classifying urban features was due to the coarse spatial resolution (79-82 meters) of Landsat MSS and the relative newness of the digital image classification technique.

However, with the improved spatial resolution of Landsat TM (30 meters), a new interest for studying urban land cover was generated. Specific to this research, Plunk, Morgan, and Newland, (1990) used the higher spatial resolution of Landsat TM to classify impervious surfaces from an urban area near Fort Worth, Texas. Their results indicated an 85.1 percent accuracy level for classifying impervious surfaces. Although both studies reported improved accuracies for classifying certain urban feature types, the authors indicated total impervious surfaces were often underestimated because of the spatial complexity and heterogeneity of many urban land covers.

After reviewing these techniques in this section, it was concluded that mapping process applies different remotely sensed data and spectral values based on the land use category. Therefore image classification using remote sensing indices was the technique chosen for this study. This was largely due to constraints in available data and manpower, but ultimately the determination is to develop a practical means by which urban areas could quantify impervious surfaces in a cost effective and timely fashion with reasonable expertise.

4. REMOTE SENSING IMAGE PROCESSING

4.1 Digital Image

Objects in the real scene can be represented by a two-dimensional image. The images can be divided in two categories, analogue and digital. Aerial photographs are examples of analogue images while satellite images acquired using electronic sensors are examples of digital images. A digital image is consisting of two-dimensional arrays of pixels, which are the picture elements and represent a square area on Earth's surface that is a measure of sensor's ability to resolve the objects of different sizes (Figure 4.1). Each pixel has brightness value, which is also called as intensity value in the digital image. Intensity value usually is a single number that represents the brightness of the pixel such as the solar radiance in a given wavelength band reflected from the ground, emitted infrared radiation or backscattered radar intensity. The most common pixel format is the byte images, where this number is stored as an 8-bit integer giving a range of possible values from 0 to 255. Typically, zero is taken to be black and 255 is taken to be white. Values in between, make up the different shades of grey.

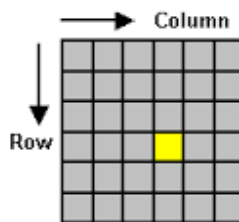


Figure 4.1 : Digital image.

4.2 Remote Sensing Spectral Indices

Spectral indices are the combinations of spectral bands at two or more wavelengths that indicate relative abundance of features of interest. There are various types of indices with different arithmetic formula used for different cases according to the characteristics of features and purpose of study.

The indices were progressed in four different stages. The first indices are those developed from simple band ratios and used for inferring the spectral properties of vegetation through its growing period. The second stage is referred to the development of indices designed to reduce the impacts of the background such as soil response. The third indices are developed to compensate for the effects of atmospheric distortion. The fourth and final stage of development procedure refers to the new spectral indices development different from vegetation health. Indices that are used for burned area assessment and fire severity are in the last developed group of indices (Harris et al, 2011). By applying the spectral indices to remotely sensed data, the sensitivity of certain surface properties is maximized. Furthermore, the indices are capable of normalizing or reducing effects due to sun angle, viewing angle, the atmosphere, topography, instrument noise, etc. to make consistent spatial and temporal comparisons possible (Jensen, 2009).

4.3 Built-up Indices

Remote sensing imagery can be used to separate urban lands from non-urban lands, but, this may not produce satisfactory accuracy because of spectral confusion of the heterogeneous urban built-up land class. Many studies have been done in combined classification methods to improve the extraction of the urban built-up lands (Xu, 2005). Transformation enhancement, one of the image - processing techniques, calculates new values for each image pixel, based not only on the values within a particular spectral band but also on some function of values in other spectral bands (Karen, 2008). Vegetation indices are ratios of bands that are designed to numerically separate or stretch the pixel value of different features in the image. Many indices have been developed that implement various band combinations. They use the distinctive feature of leaf chlorophyll absorption (maximum at about 0.69 μm) and lack of absorption in the adjacent near infrared region (at 0.85 μm) to isolate different features. The outcome is a strong absorption contrast in the 0.65 - 0.85 μm wavelength interval (Liwa, 2006). Vegetation indices utilise this contrast through the combinations of bands red/near-infrared reflectance. There are a number of vegetation indices, such as the Normalized Difference Vegetation Index (NDVI), that are function of the visible bands of multispectral data and the near infrared bands. It has been determined that these indices often give a very simple and fast interpretation of Landsat satellite data in terms of

vegetation health. Likewise, there are other indices using different spectral bands that may be calculated to allow more efficient interpretation of features (Kemp, 2008).

The mapping process applies different remotely sensed data and spectral values based on the land use category. Land use mapping primarily employs the multispectral classification method; however, there are other methods that also utilise the application of the remote sensing index. Chen et al. (2006) classified urban land uses using several remote sensing indices in the Pearl River Delta of China with high accuracy. The most popular indices which are relatively good for mapping the impervious surface and bare land in urban areas, such as the Normalised Difference Built-Up Index (NDBI) Zha et al. (2003), Index-based Built-Up Index (IBI) Xu, (2008), Urban Index (UI) Kawamura et al. (1996), Normalised Difference Bareness Index (NDBaI) Zhao and Chen (2005), and Bare soil index (BI) Rikimaru and Miyatake (1997), Enhanced Built-Up and Bareness Index (EBBI) As-syakur et al. (2012) have been employed in various studies. The IBI, NDBI, UI, and EBBI are indices for quickly mapping impervious surface and bare land areas. In contrast, the NDVI is a well-known spectral index for rapidly mapping the distribution of vegetation and a variety of conditions over land surfaces. Previously, Braun and Herold (2004) applied NDVI for mapping the impervious area of an urban area of Germany.

In the following built-up and bare land indices which was used in this study for Landsat 5 TM are explained and presented in Table 5.6 and for Landsat 8 OLI & TIRS in Table 5.7.

4.3.1 Normalised difference built-up index (NDBI)

Zha et al. (2003) suggested that spectral disparity is the largest in bands 3, 4 and 5 of landsat 5 TM. An examination of the minimum, maximum and standard deviation of each of the covers in the seven TM bands confirms the same conclusion. Namely, these values are most distinctive from one another for each cover in bands 3, 4 and 5. Therefore, they are the most useful bands from which some of the land covers may be potentially differentiated spectrally. Rivers and lakes have a similar shape of profile. Their Digital Number (DN) value is markedly lower in the fourth and fifth bands. They experience a sharp rise in reflectance in band 6, but a low reflectance in band 7. The curve for rivers lies above that for lakes because they are laden with more silt. A close look reveals that except for barren, vegetation (woodland and farmland) has a higher

reflectance on band 4 than other covers. Moreover, its value on band 4 still exceeds those on band 3. By comparison, all the non-vegetative categories have a smaller DN on band 4 than 3. Therefore, the subtraction of band 3 from band 4 will result in positive DNs for vegetation pixels only. The aforementioned relationships exist for the minimum and maximum DNs as well . This outcome allows broad vegetative covers to be distinguished easily. This processing is commonly referred to as NDVI .

$$\text{NDVI} = (\text{Band 4} - \text{band 3}) / (\text{band 4} + \text{band 3}) \quad (4.3)$$

In order to facilitate the subsequent processing, the derived NDVI image was recoded with 254 for all pixels having positive indices (vegetation) and 0 for all remaining pixels of negative indices. Impervious surface areas and barren land experience a drastic increment in their reflectance from band 4 to band 5 while vegetation has a slightly larger or smaller DN value on band 5 than on band 4. This pace of increment greatly exceeds that of any other covers. The minimum and maximum DNs in band 4 are much smaller than those in band 5 for the same cover. The standardized differentiation of these two bands (equation 4.4) will result in close to 0 for woodland and farmland pixels, negative for waterbodies, but positive values for impervious surface pixels, enabling the latter to be separated from the remaining covers.

$$\text{NDBI} = (\text{band 5} - \text{band 4}) / (\text{band 5} + \text{band 4}) \quad (4.4)$$

4.3.2 Normalized difference bareness index (NDBaI)

Normalized Difference Bareness Index (NDBaI) was first introduced by Zhao and Chen in 2004. This index is based on significant differences of spectral signature in the near-infrared (band 5 landsat 5 TM) between the bare-soil and the backgrounds. However, it showed little difference between impervious surface areas and bare-soil areas in band 5 (Figure 4.2) (Zhao and Chen, 2004). Figure 4.2 suggests that further consideration of the visible may be necessary to determine the vegetation areas. It is effective in distinguishing bare-soil from similarly impervious surface and vegetation.

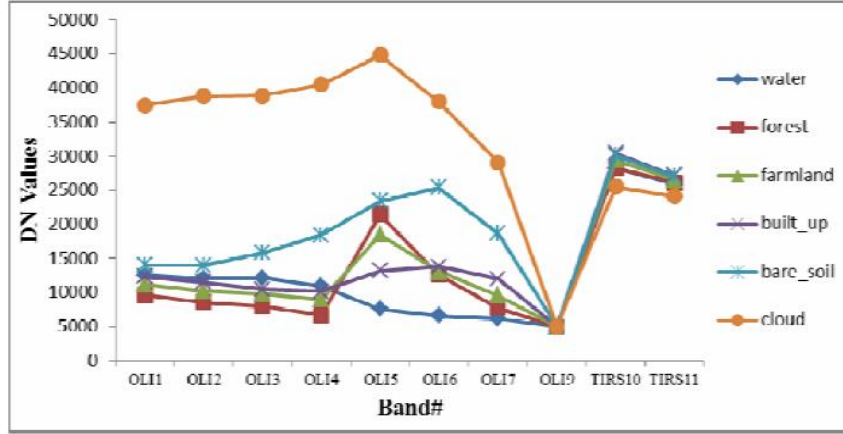


Figure 4.2 : Spectral profiles of six typical land covers for Landsat8 OLI & TIRS

$$NDBaI = \frac{Band5 - Band6}{Band5 + Band6} \quad (4.5)$$

4.3.3 Index-based built-up index (IBI)

An urban area is a complex ecosystem composed of heterogeneous materials. Nevertheless, based on some generalizing features, Ridd (1995) could still divide the urban ecosystem into three components, green vegetation, impervious surface material and exposed soil, and accordingly created a V-I-S model.

Consequently, the urban land-use was grouped into three other generalizing categories: built-up land, vegetation and open water. Based on these three components, three thematic indices, the normalized difference built-up index (NDBI), the soil adjusted vegetation index (SAVI) and the modified normalized difference water index Xu (2006), were selected to represent the three major land-use classes respectively.

$$NDBI = \frac{(Band 5 - Band 4)}{(Band 5 + Band 4)} \quad (4.6)$$

$$SAVI = \frac{(Band 4 - Band 3)(1 - l)}{(Band 4 + Band 3 + l)} \quad (4.7)$$

$$MNDWI = \frac{(Band 2 - Band 5)}{(Band 2 + Band 5)} \quad (4.8)$$

The selection of the SAVI instead of the NDVI is because the SAVI is more sensitive than the NDVI in detecting vegetation in the low-plant covered areas such as urban areas. The SAVI can work in the area with plant cover as low as 15%, while the NDVI can only work effectively in the area with plant cover above 30% (Ray, 2006).

Therefore, the SAVI is more suitable for the urban area. However, in the area where the plant cover is more than 30%, the NDVI can be used:

$$NDVI = \frac{(Band\ 4 - Band\ 3)}{(Band\ 4 + Band\ 3)} \quad (4.9)$$

After producing SAVI, MNDWI, and NDBI images, a new image is created, which used these three new images as three bands. The change from the original multi-band image into the three-thematic-band image largely reduces redundancy between original multi-spectral bands, and the three new bands are negatively correlated with each other. Consequently, the spectral clusters of the three major urban components are well separated. According to these distinct features, the IBI can be created as follows:

$$IBI = \frac{[NDBI - (SAVI + MNDWI)/2]}{[NDBI + (SAVI + MNDWI)/2]} \quad (4.10)$$

Obviously, the IBI is a normalized difference index and thus has such features as: (1) a ratio-based index, (2) values ranging from -1 to + 1 and (3) enhanced information has positive values, while the unwanted background noise generally has zero to negative values. Dividing by two in the equation is to avoid getting too small values of IBI. Before calculating the IBI using equation (4.10), the values of the NDVI, the NDBI and the MNDWI should be added to 1 or rescaled within 0–255 to convert negative values of the indices into positive values.

The IBI is distinguished from conventional indices by its first-time use of thematic index-derived bands, instead of original image bands, to construct an index. When the NDVI is used instead of the SAVI in equation (4.10), the IBI can be rewritten, based on equations (4.6), (4.7), (4.8) and (4.10), as:

$$IBI = \frac{2MIR/(MIR+NIR) - [NIR/(NIR+Red) + Green/(Green+MIR)]}{2MIR/(MIR+NIR) + [NIR/(NIR+Red) + Green/(Green+MIR)]} \quad (4.11)$$

or

$$IBI = \frac{\frac{2Band5}{Band5+Band\ 4} - \left[\frac{Band4}{Band4+Band3} + \frac{2}{Band2+Band5} \right]}{\frac{2Band5}{Band5+Band\ 4} + \left[\frac{Band4}{Band4+Band3} + \frac{2}{Band2+Band5} \right]} \quad (4.12)$$

4.3.4 Urban index (UI)

Urban Index (UI) was first proposed by Kawamura et al. (1996) based on computing using Landsat5 TM band7 (B7) and band4 (B4), exploiting an observed inverse

relationship between the brightness of urban areas in the near infrared (0.76 μm – 0.90 μm) and mid infrared (2.08 μm – 2.35 μm) portions of spectrum.

$$UI = \frac{\text{Band7}-\text{Band4}}{\text{Band7}+\text{Band4}} \quad (4.13)$$

This index was verified by examining its relation with the normalised difference vegetation Index (NDVI), land cover and building cover data. The UI-NDVI relation shows that the UI value increases and NDVI value decreases with increased urbanization.

4.3.5 Enhanced built-up and bareness index (EBBI)

The EBBI As-syakur et al. (2012) is a remote sensing index that applies wavelengths of 0.83 μm , 1.65 μm , and 11.45 μm , (NIR, SWIR, and TIR, respectively) to Landsat ETM+ images. These wavelengths were selected based on the contrast reflection range and absorption in impervious surface and bare land areas. According to Herold *et al.*, the reflectance values of impervious surface areas are higher due to the longer sensor wavelengths. The NIR wavelength, which corresponds to band 4 in Landsat ETM+ and band 5 in SWIR, is associated with a high contrast level for detecting impervious surface and bare land areas. In addition, in bands 4 and 5, there is an obverse reflectance ratio with respect to detecting impervious surface or bare land areas compared to vegetation. Vegetation has a high reflectance in band 4, but the reflectance of impervious surface or bare land in band 4 is low. In contrast, in band 5, there is high reflectance when detecting impervious surface areas compared with vegetated areas. NIR and SWIR were used for mapping impervious surface areas in a study conducted by Zha et al. (2004) when developing the NDBI index.

Zhao and Chen (2005) utilized Landsat ETM+ band 5 (SWIR) and band 6 (TIR) to generate the NDBaI. The NDBaI is an index used to map bare land areas. The TIR can distinguish high and low levels of albedo in impervious surfaces. According to Weng (2008), the utilization of TIR channels is very effective for mapping impervious surface areas based on a low albedo, which eliminates the effect of shadows and water, while a high albedo demonstrates impervious surface and bare land areas clearly. The TIR channel also exhibits a high level of contrast for vegetation. The temperature of a impervious surface area is 10–12 degrees higher than that of vegetation. Therefore, the combination of NIR, MIR, and TIR (Landsat ETM+ bands 4, 5, and 6) wavelengths

makes it possible to improve the mapping method for impervious surface and bare land areas relative to previously existing remote sensing indices.

By combining the NIR, MIR, and TIR (Landsat ETM+ bands 4, 5, and 6) wavelengths, the subtraction of band 4 from band 5 will result in positive values for impervious surface and barren pixels and will result in negative values for vegetation. In addition, a summation of band 5 and band 6 will result in higher values pixel for impervious surface and bare land than for vegetation. The difference between the subtraction of band 4 from band 5 and the summation of band 5 and band 6 will result in virtually 0 water pixels as well as negative values for vegetation and positive values for impervious surface and barren pixels. This outcome allows for easy distinguishing between impervious surface and bare land areas.

To achieve a higher level of contrast, an improvement in the mathematical operations was introduced into the equation used to calculate the EBBI. The EBBI applies a root function to distinguish the numbers that represent similar objects based on the different levels of reflectance values. To obtain an index value of -1~1, the multiplied factor is divided by ten. The EBBI is calculated from the image data using the following formula:

$$EBBI = \frac{\text{Band 5} - \text{Band 4}}{10\sqrt{\text{Band 5} + \text{Band 6}}} \quad (4.14)$$

4.4 Image Classification

Image classification is the process to produce thematic maps from imagery. The themes can range from different categories such as soil, vegetation and water in general or in more detailed description type of soils, vegetation and water depths. The most important factor in creating thematic map from remotely sensed imagery is that the categories selected for the map should be distinguishable in the image.

Electromagnetic radiation reflected by similar objects on the Earth's surface can have similar spectral properties. The goal of classification is to identify homogeneous groups of pixels with similar spectral signature, and based on their spectral information represented by the digital numbers, classify them in different groups or classes and by this process make it possible to model the Earth's surface. Different methods have been developed to classify digital images by spectral properties of the objects present in the image.

4.5 Density Slicing

One of the most common and simple image processing routine for information extraction is density slicing. Density slicing is the process in which the pixel values are sliced into different ranges and for each range, a single value or colour is assigned in the output image. It is also known as level slicing and works best on single band images. It is especially useful when a given surface features has a unique and generally, narrow set of DN values (Figure 4.3).

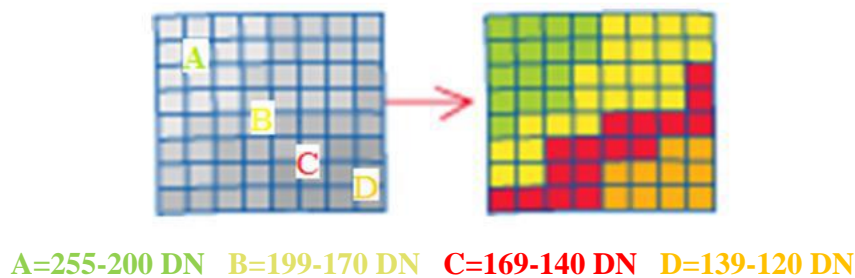


Figure 4.3 : Density slicing.

For example, in a black-and-white thermal image the temperature values in the image can be split into bands of 2°C, and each band represented by a colour of the spectrum. Therefore the temperature information in the image can be analysed more easily because the differences between the colours are greater than the black and white and therefore it is easier to analyse the data contained in the image.

4.6 Accuracy Assessment

Accuracy indicates that how well the classified images identifies the land cover type on the ground. The accuracy of a classification is usually assessed by comparing the classification with some reference data that is believed to accurately reflect the true land cover. Sources of reference data include among other things ground truth, higher resolution satellite images, and maps derived from aerial photo interpretation. Accuracy assessment should not be based on the training pixels. The problem with using training pixels is that they are usually not randomly selected, and that the classification is not independent of the training pixels. Using training pixels usually results in an overly optimistic accuracy assessment. The results of an accuracy assessment are usually summarized in a confusion matrix (Foody, 2002) .

The error matrix is currently at the core of the accuracy assessment literature. As a simple cross-tabulation of the mapped class label against that observed in the ground or reference data for a sample of cases at specified locations, it provides an obvious foundation for accuracy assessment (Campbell, 1996). The columns of an error matrix contain the reference data and the rows represent the results of the remote sensed classified data. This is an effective way to represent accuracy of each classified category (Figure 4.4).

| | | Actual Class | | | | |
|-----------------|----------|--------------|----------|----------|----------|----------|
| | | A | B | C | D | Σ |
| Predicted Class | A | n_{AA} | n_{AB} | n_{AC} | n_{AD} | n_{A+} |
| | B | n_{BA} | n_{BB} | n_{BC} | n_{BD} | n_{B+} |
| | C | n_{CA} | n_{CB} | n_{CC} | n_{CD} | n_{C+} |
| | D | n_{DA} | n_{DB} | n_{DC} | n_{DD} | n_{D+} |
| | Σ | n_{+A} | n_{+B} | n_{+C} | n_{+D} | n |

Figure 4.4 : The error matrix (Foody, 2002)

The error matrix is a multidimensional table, its cells contain change data from a category to another. The statistical approach of the accuracy assessment consists of different multivariate statistical analysis. The highlighted elements represent the main diagonal of the matrix that contains the cases where the class labels depicted in the image classification and ground data set agree, whereas the off-diagonal elements contain those cases where there is a disagreement in the labels. Accuracy assessment measures are overall accuracy and KAPPA (Cohen, 1960). KAPPA is designed to compare results from different regions or different classifications.

The KAPPA equation is:

$$\hat{K} = \frac{N \sum_{i=1}^n X_{ii} \sum_{i=1}^n (X_{i+} * X_{+i})}{N^2 \sum_{i=1}^n (X_{i+} * X_{+i})} \quad (4.15)$$

Overall accuracy equation is:

$$\text{Overall accuracy} = \frac{\sum_{i=1}^n X_{ii}}{n} \times 100 \quad (4.16)$$

Where

n is the number of rows in the matrix,

X_{ii} = number of observations in the row i and column I ,

X_{i+} = the marginal totals of row i and column I ,

N = total number of observations.

5. STUDY AREA , DATA AND CASE STUDY

The effectiveness of remote sensing data in estimation of impervious surface and bare land area and its accuracy was examined by using Landsat 5 TM and Landsat 8 OLI & TIRS with 30 meters spatial resolution.

5.1 Study Area

Istanbul is located between longitudes 27° 58' and 29° 56' E and latitudes 40° 48' and 41° 36' N in northwest of turkey (Kurt, 2012). Istanbul is the biggest city of Turkey with the population over 14.6 milion according to the Turkish Statistic Institute (2015), showing an astonishing increase compared to 4.7 milion according to 1980 census reports. In 1980, there were 19 districts inside Istanbul province borders; but covering a total area of approximately 5,750 km², management difficulties and political reasons led the province to to be devided into 39 districts (Kaya et al, 2014). It is surrounded by the Black Sea in the north and the Sea of Marmara in the south. It is divided into two parts by The Bosphorus Strait to be one in Asia and one in Europe (Balik Sanli, 2011). 25 of these districts were located in European side while 14 of them are located in Anatolian side of Istanbul (Figure 5.1).

The land cover change occurred in Istanbul affect environment in some main fields: Impacts on forest areas and natural grassland, on the water reservoir storage, on soil and coastal and on the climate (Bektas Balcik, 2013). There are so many studies concerning the impacts of land cover change in Istanbul and come with certain results. According to a study in this region by Musaoglu et al. (2006) there is a decline of forest areas resulted from establishment of new residential areas and illegal constructions within forest areas.

New megaprojects such as a third bridge on the Bosphorus and a third international airport near the northern forest region which will be located mainly on the Black Sea coastal area of the city facing Europe will be the main threats to the natural resources of the city, in the near future. These formerly vegetated areas will be replaced mostly

by artificial surfaces when the projects are completed (Bektas Balcik, 2013). A third bridge built on the Bosphorus will obviously transform 40 % of the forest areas and 83 % of the bare and agricultural lands located in the northern part of the city into artificial settlement areas (Ayazli, 2011).

Climate is other factor affected by land cover change. A study by Sertel and Ormeci (2009) in the Marmara Region, which experienced significant land cover changes as a result of rapid industrialization and population increase especially after 1980s, reveal that anthropogenic land cover change has impacted several aspects of the regional climate of the Marmara Region, including warming of 2° C air temperatures and the changes in the strength and orientation of the sea breezes. Urbanization increase in Istanbul resulted in urban heat island effect over this city (Bektas Balcik, 2013). Climate change adversely affect animal, human, agriculture and ecosystems.

All in all, the megacity Istanbul is the economical capital of Turkey and the city has been under the pressure of rapid and unplanned urbanization. Monitoring urban growth and land cover change will enable the greater Istanbul metropolitan municipality for a better management of this complex urban area (Geymen and Baz, 2008).



Figure 5.1 : Location of the Istanbul

5.2 Data Used

In this study, the Landsat 5 TM (20.08.2003) and Landsat 8 OLI & TIRS (06.09.2015) satellite images with 30-meter spatial resolution were used.

5.2.1 Remote sensing satellites

A satellite is an object that orbits around a larger object. As an example, the moon is a satellite because it orbits around the Earth, but there are many artificial and man-made satellites, which are launched into space and can orbit the Earth for different purposes. Some satellites are used for taking images from other planets or the Earth's surface and some other satellites are used in communication. There are so many satellites with

different characteristics from different countries. Among all the satellites, Landsat Thematic Mapper (TM), Landsat Multispectral Scanner System (MSS), Landsat Enhanced Thematic Mapper Plus (ETM⁺), Landsat Operational Land Imager (OLI) are freely available for mapping impervious surface and bare land area as multispectral satellites sensor with mid-resolution. Because of the presence of short wave infrared and long wave infrared among the bands of these satellites that are more advantageous in Impervious surface, soil and vegetation based studies, Landsat can be categorized as a most preferred satellite for impervious surface mapping (Xu, 2008).

5.2.2 Landsat system

Landsat satellites were first launched in 1972 with Landsat 1. For 40 years, the Landsat satellites have provided scientists with continuous data and variety of characteristics that has contributed to human knowledge of the water cycle, climate, ecosystems, and the changing Earth and more.

5.2.3 Characteristics of Landsat

In the last half century deliberating of environmental change over the time was possible for scientist using Landsat satellite. The continuous global record, medium spatial resolution and the opening of the Landsat archives to the public in 2008 has made this dataset one of the most prevalent in Earth system studies (Landsat 7 Science Data Users Handbook, 2006).

Overall there are 6 Landsat satellites from beginning up to now, Landsat 1-3, Landsat 4-5, Landsat 7 and Landsat 8. Each of Landsat satellites has their own characteristics and these are given in the next section.

5.2.3.1 Sensors and specifications

MSS (Multi Spectral Scanner), TM (Thematic Mapper), ETM (Enhanced Thematic Mapper), ETM⁺ and OLI (Operational Land Imager) sensors can be named as Landsat satellite system's sensors.

The Landsat Multispectral Scanner (MSS) sensor was on board Landsat 1 through 5, and acquired images of the Earth nearly continuously from July 1972 and collected data until January 2013 when the mission of Landsat 5 was expired. MSS data was

acquired with a 6-bit system and has 80-meter spatial resolution while TM and ETM⁺ acquire data in an 8-bit system.

TM sensor has spatial resolution of 30 meter with 6 bands in NIR and SWIR portion of spectrum while the Thermal band has 120 meter resolution. Specific technical information of Landsat 5 TM is given in the Table 5.1 and Table 5.2.

Table 5.1 : Technical information of Landsat 5 TM.

| Properties | Description |
|----------------|---|
| Operator | U.S. Geological Survey (USGS) |
| Launch date | 1-Mar-84 |
| Altitude | 705 km (438 mi) |
| Life time | 5 years |
| Orbit | Sun-synchronous, Near-polar |
| Slope of orbit | 98.2 |
| Quantization | 8 bit (256 levels) |
| Swath width | 185 km (115 mi) |
| Repeat cycle | 16 days |
| Sensors | MSS (Multi Spectral Scanner) TM (Thematic Mapper) |

Table 5.2 : Characteristics of Landsat 5 TM.

| Band | Resolution (m) | Wavelength (μm) | Description |
|------|-------------------|---------------------------------|---------------------|
| 1 | 30 | (0.45-0.52) | Blue |
| 2 | 30 | (0.52-0.60) | Green |
| 3 | 30 | (0.63-0.69) | Red |
| 4 | 30 | (0.76-0.90) | Near Infrared |
| 5 | 30 | (1.55-1.75) | Short wave Infrared |
| 6 | 120 | (10.4-12.5) | Thermal Infrared |
| 7 | 30 | (2.08-2.35) | Short wave Infrared |

OLI and TIRS are two sensors of Landsat 8 Earth-observation satellite as a last part of the Landsat Data Continuity Mission. The technical information of Landsat 8 OLI & TIRS is given in Table 5.3 and Table 5.4 (Landsat 8 (L8) data users handbook, 2016).

Table 5.3 : Technical information of Landsat 8 OLI & TIRS.

| Properties | Description |
|----------------|---|
| Operator | U.S. Geological Survey (USGS) |
| Launch date | 11 February 2013 |
| Altitude | 705 km (438 mi) |
| Life time | 5-6 years |
| Orbit | Sun-synchronous Near-polar |
| Slope of orbit | 98.2 |
| Quantization | 12 bit(4096 levels) |
| Swath width | 185 km (115 mi) |
| Repeat cycle | 16 days |
| Sensors | OLI (Operational Land Imager) TIRS (Thermal Infrared Sensor) |

Table 5.4 : Characteristics of Landsat 8 OLI & TIRS.

| Band | Resolution (m) | Wavelength (μm) | Description |
|------|-------------------|---------------------------------|---------------------|
| 1 | 30 | (0.43-0.55) | Coastal aerosol |
| 2 | 30 | (0.45-0.51) | Blue |
| 3 | 30 | (0.53-0.59) | Green |
| 4 | 30 | (0.64-0.67) | Red |
| 5 | 30 | (0.85-0.88) | Near Infrared |
| 6 | 60 | (1.57-1.65) | Short wave Infrared |
| 7 | 30 | (2.11-2.29) | Short wave Infrared |
| 8 | 15 | (0.50-0.68) | Panchromatic |
| 9 | 30 | (1.36-1.38) | Cirrus |
| 10 | 100(30) | (10.60-11.19) | Thermal Infrared |
| 11 | 100(30) | (11.50-12.51) | Thermal Infrared |

Comparing to Landsat 5 TM, Landsat 8 OLI & TIRS has several new features and improvements (Jia et al, 2014) :

- Having two OLI and TIRS sensors.
- A deep blue visible channel (band 1) specifically designed for water resources and coastal zone investigation.

- A new infrared channel (band 9) for the detection of cirrus clouds.
- The TIRS instrument collects two spectral bands for the wavelength covered by a single band on the previous TM and ETM⁺ sensors.
- Improvement of the spectral responses across the channels by a refined spectral range for some bands, e.g. near-infrared (NIR) and panchromatic bands.
- The data quality (signal to noise ratio) and radiometric quantization (12-bits) of the OLI and TIRS is higher than previous Landsat instruments (8-bit for TM and ETM⁺), providing significant improvement in the ability to detect changes on the Earth's surface.
- A new Quality Assurance band is also included with each data product. This provides information on the presence of features such as clouds, water, and snow.
- To avoid the effect of water vapour absorption NIR band is narrowed at 0.825 μm , similar to that of MODIS, and helps acquire accurate surface reflectance.
- Spectral record precision is improved by enhancing the radiometric resolution to avoid the spectral saturation comparing to previous Landsat data.

Consequently, the Landsat 8 OLI & TIRS data are anticipated to perform better for in land cover mapping.

Data for this study is downloaded from the US Geologic survey's Earth Explorer database (<http://earthexplorer.usgs.gov>) for two different dates. The dates of satellite images used are given in the Table 5.5.

Table 5.5 : The dates of Landsat data used

| LANDSAT 5 TM | LANDSAT 8 OLI & TIRS |
|--------------|----------------------|
| 20.8.2003 | 06.09.2015 |

Data set consists of two Landsat images belonging to years 2003 and 2015 summer cropping season. Since the study area is covering two frames of Landsat satellite (180/31 and 180/32), both frames of scene are downloaded and are mosaicked and then subsetting to Istanbul boundaries using ENVI software (5.2) to create a whole scene of the study area (Figure 5.2).

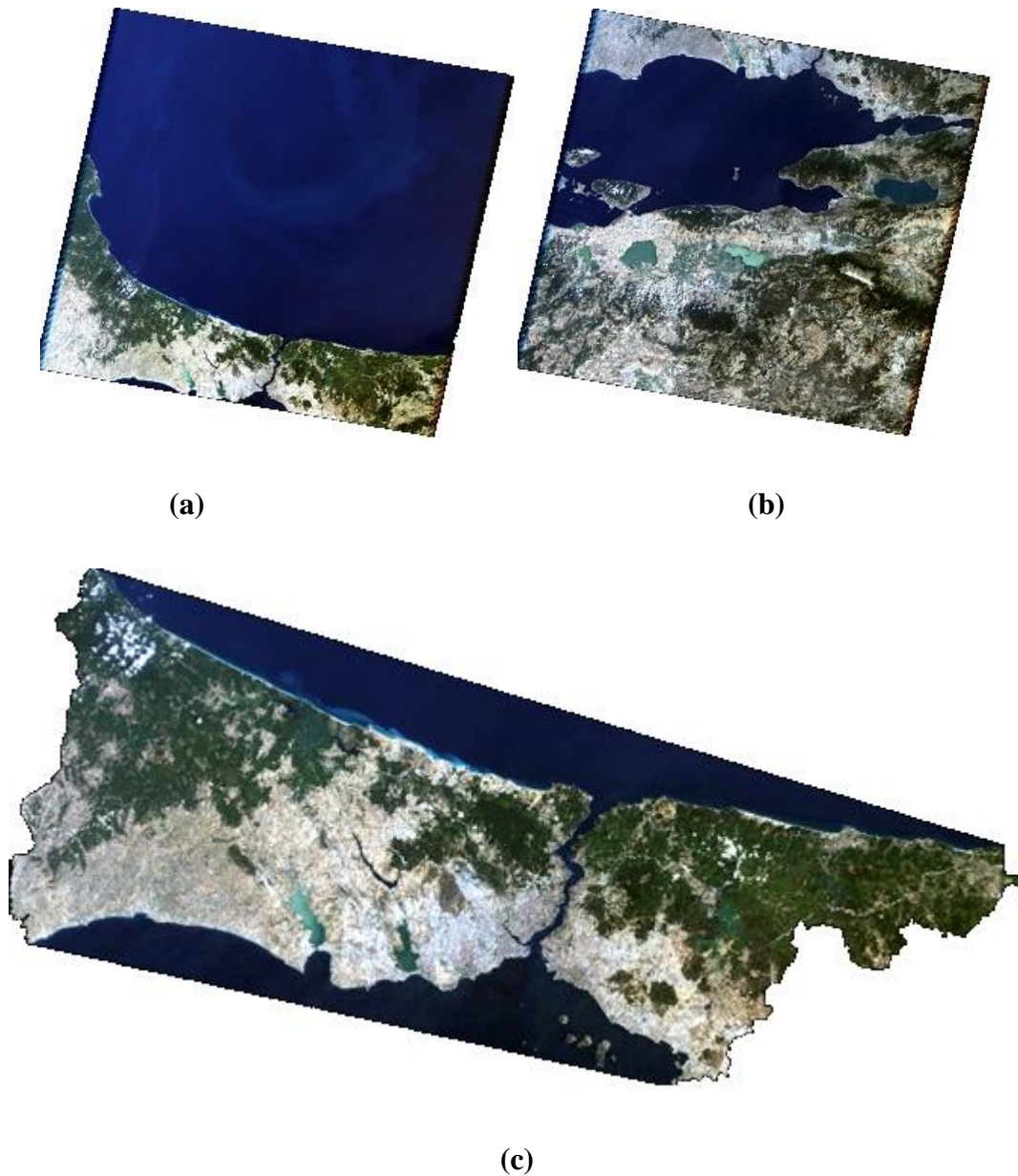


Figure 5.2 : Landsat 5 TM - 20/08/2003 data (a) Frame 180/ 31 (b) Frame 180/ 32 (c) Mosaic and subsetting image.

5.3 Spectral Indices

5.3.1 Built-up area indices

Various spectral built-up indices developed in numerous studies related to impervious surface and bare land area detection and mapping, are summarized in section 4.4. In this study, all different built-up indices represented in table 5.6 and 5.7 are examined for all the Landsat images from years 2003 to 2015 and the result of built-up indices are given in the Figure 5.4, Figure 5.5, Figure 5.6, Figure 5.7 and 5.8.

Table 5.6 : Extracted urban indices from Landsat5 TM imagery.

| Name of Urban Index | Abbreviation | Equation | Reference |
|--------------------------------------|--------------|---|-------------------------|
| Enhanced Built-Up and Bareness Index | EBBI | $EBBI = \frac{\text{Band 5} - \text{Band 4}}{10\sqrt{\text{Band 5} + \text{Band 6}}}$ | (As-syakur et al, 2012) |
| Index-based Built-Up Index | IBI | $IBI = \frac{\frac{2\text{Band 5}}{\text{Band 5} + \text{Band 4}} - \left[\frac{\text{Band 4}}{\text{Band 4} + \text{Band 3}} + \frac{\text{Band 2}}{\text{Band 2} + \text{Band 5}} \right]}{\frac{2\text{Band 5}}{\text{Band 5} + \text{Band 4}} + \left[\frac{\text{Band 4}}{\text{Band 4} + \text{Band 3}} + \frac{\text{Band 2}}{\text{Band 2} + \text{Band 5}} \right]}$ | (Xu, 2008) |
| Normalized Difference Build-up Index | NDBI | $NDBI = \frac{(\text{Band 5} - \text{Band 4})}{(\text{Band 5} + \text{Band 4})}$ | (Zha et al, 2003) |
| Urban Index | NDBaI | $NDBaI = \frac{\text{Band 5} - \text{Band 6}}{\text{Band 5} + \text{Band 6}}$ | (Kawamura et al, 1996) |
| Normalized Difference Bareness Index | UI | $UI = \frac{\text{Band 7} - \text{Band 4}}{\text{Band 7} + \text{Band 4}}$ | (Zhao and Chen, 2005) |

Abbreviation used in equations:

Band2= Green; Band3= Red; Band4= Near-Infrared; Band5= Near-Infrared; Band6= Thermal; Band7= Mid-Infrared

Table 5.7 : Extracted urban indices from Landsat8 OLI & TIRS imagery.

| Name of Urban Index | Abbreviation | Equation | Reference |
|--------------------------------------|--------------|---|-------------------------|
| Enhanced Built-Up and Bareness Index | EBBI | $EBBI = \frac{\text{Band 6} - \text{Band 5}}{10\sqrt{\text{Band 6} + \text{Band 10}}}$ | (As-syakur et al, 2012) |
| Index-based Built-Up Index | IBI | $IBI = \frac{\frac{2\text{Band 6}}{\text{Band 6} + \text{Band 5}} - \left[\frac{\text{Band 5}}{\text{Band 5} + \text{Band 4}} + \frac{\text{Band 3}}{\text{Band 3} + \text{Band 6}} \right]}{\frac{2\text{Band 6}}{\text{Band 6} + \text{Band 5}} + \left[\frac{\text{Band 5}}{\text{Band 5} + \text{Band 4}} + \frac{\text{Band 3}}{\text{Band 3} + \text{Band 6}} \right]}$ | (Xu, 2008) |
| Normalized Difference Build-up Index | NDBI | $NDBI = \frac{(\text{Band 6} - \text{Band 5})}{(\text{Band 6} + \text{Band 5})}$ | (Zha et al, 2003) |
| Urban Index | NDBaI | $NDBaI = \frac{\text{Band 6} - \text{Band 10}}{\text{Band 6} + \text{Band 10}}$ | (Kawamura et al, 1996) |
| Normalized Difference Bareness Index | UI | $UI = \frac{\text{Band 7} - \text{Band 5}}{\text{Band 7} + \text{Band 5}}$ | (Zhao and Chen, 2005) |

Abbreviation used in equations:

Band3= Green; Band4= Red; Band5= Near Infrared; Band6= Short-wave Infrared (SWIR) 1; Band7= Short-wave Infrared (SWIR) 2; Band10= Thermal Infrared (TIRS) 1

Method

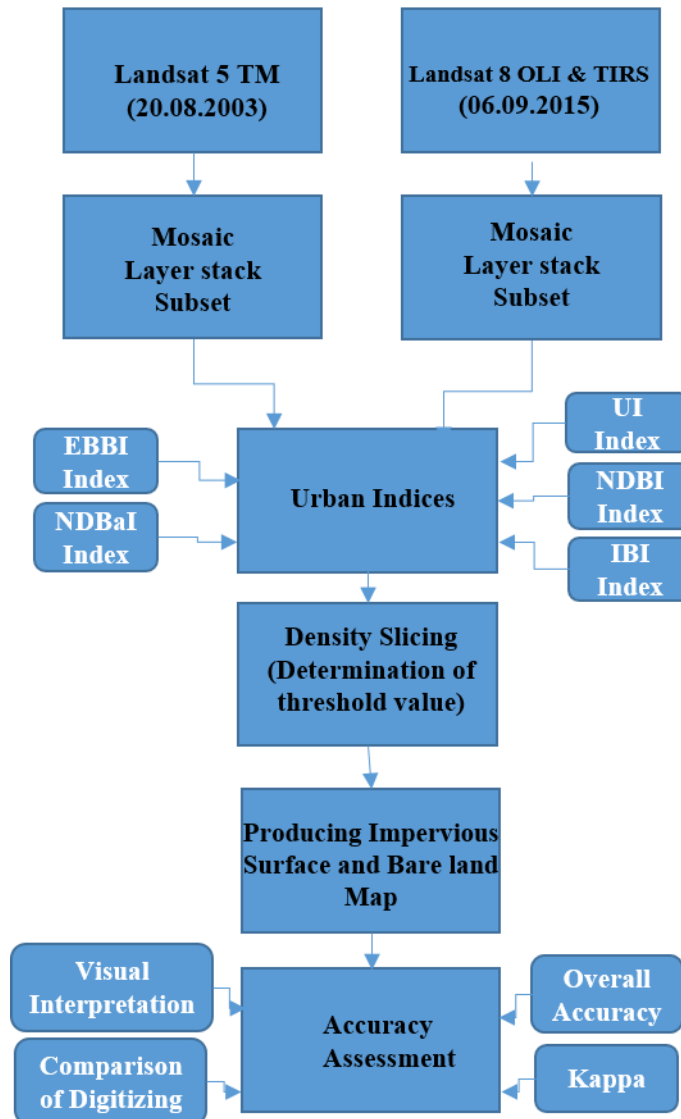
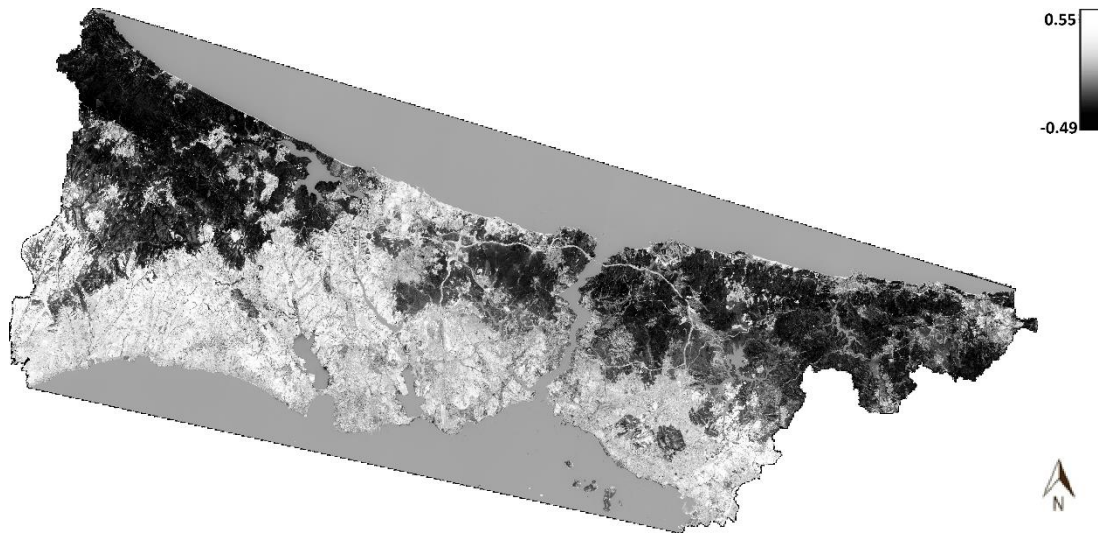
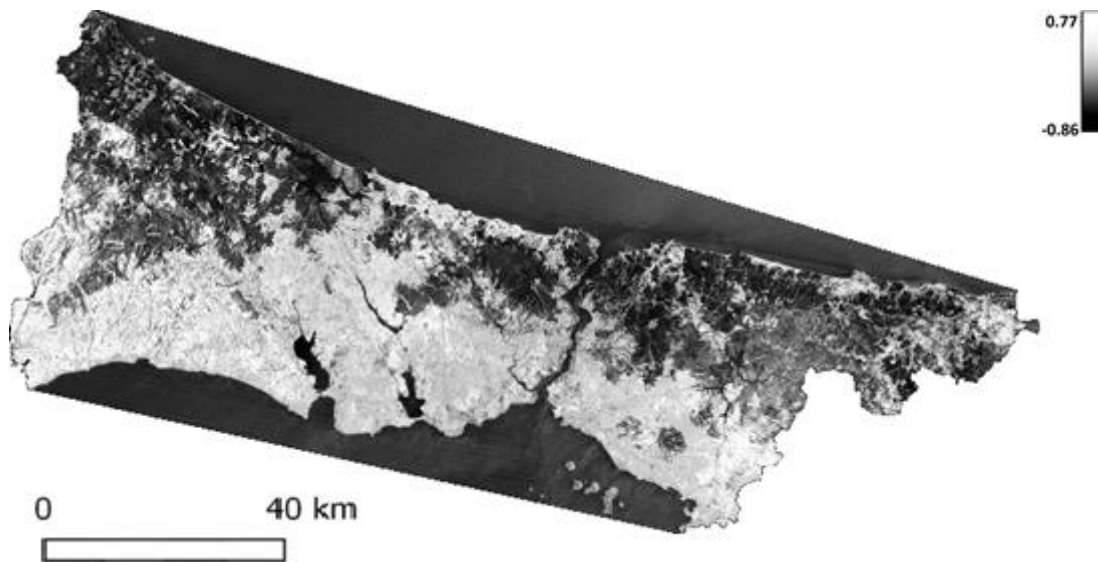


Figure 5.3 : Flowchart of estimating impervious surface and bare land fraction in the study.



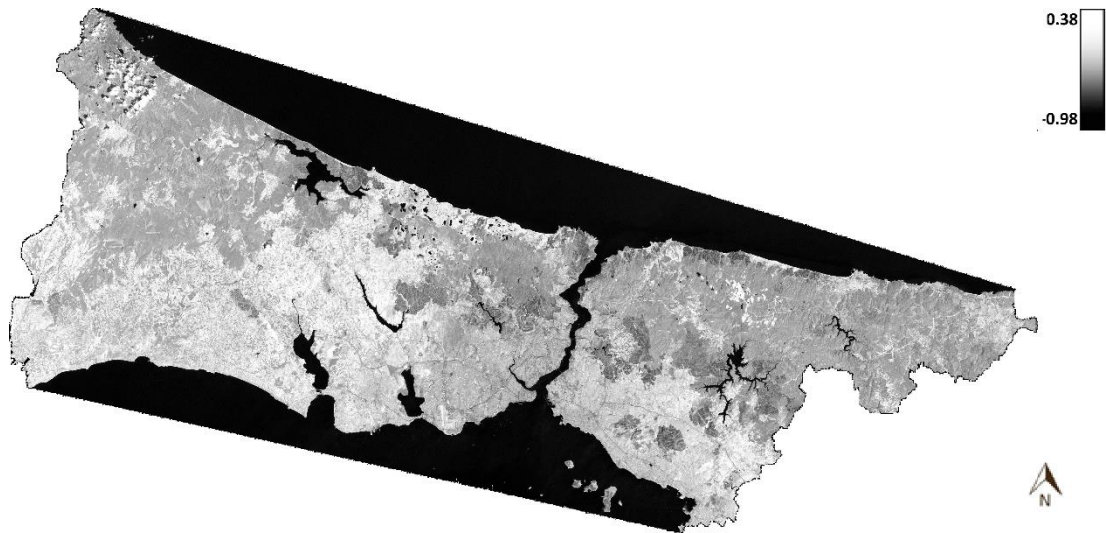
(a)



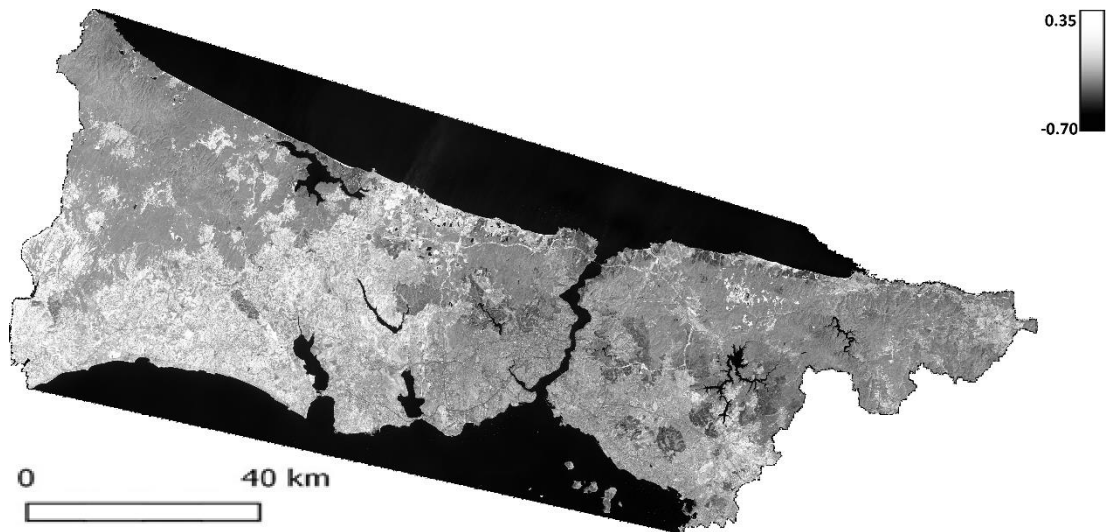
(b)

Figure 5.4 : NDBI images of Istanbul (a) August 20, 2003 (b) September 06, 2015

As observable from NDBI images, impervious surface areas with higher NDBI values are shown by brighter colours while the surfaces with low imperviousness are shown by darker colours. this is a result of the minimum and maximum DNs in band 4 are much smaller than those in band 5 for the same cover. The standardized differentiation of these two bands will result in close to zero for forest and farmland pixels, negative for water surfaces, but positive values for built-up pixels, enabling the latter to be separated from the remaining covers.

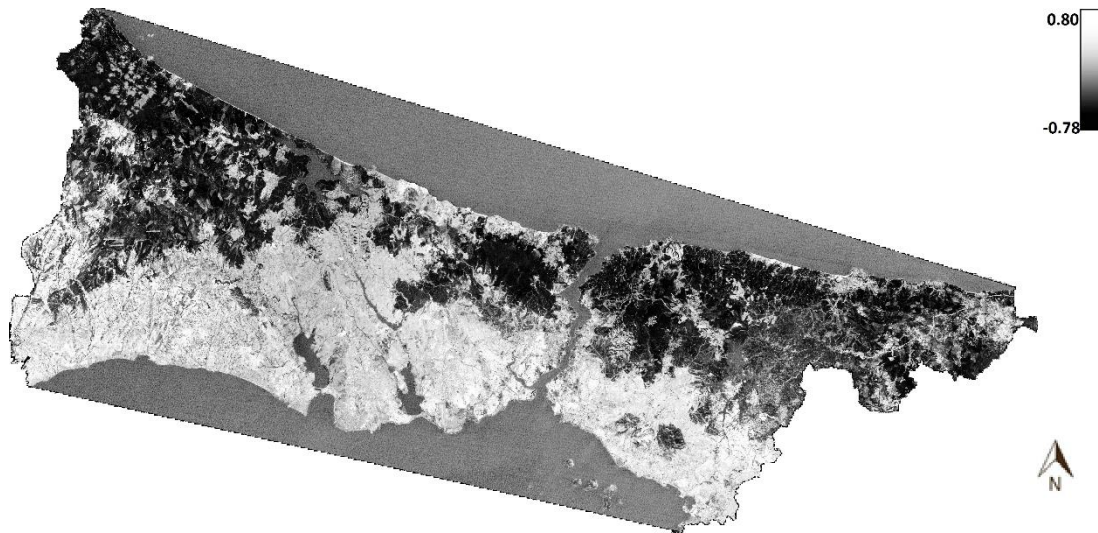


(a)

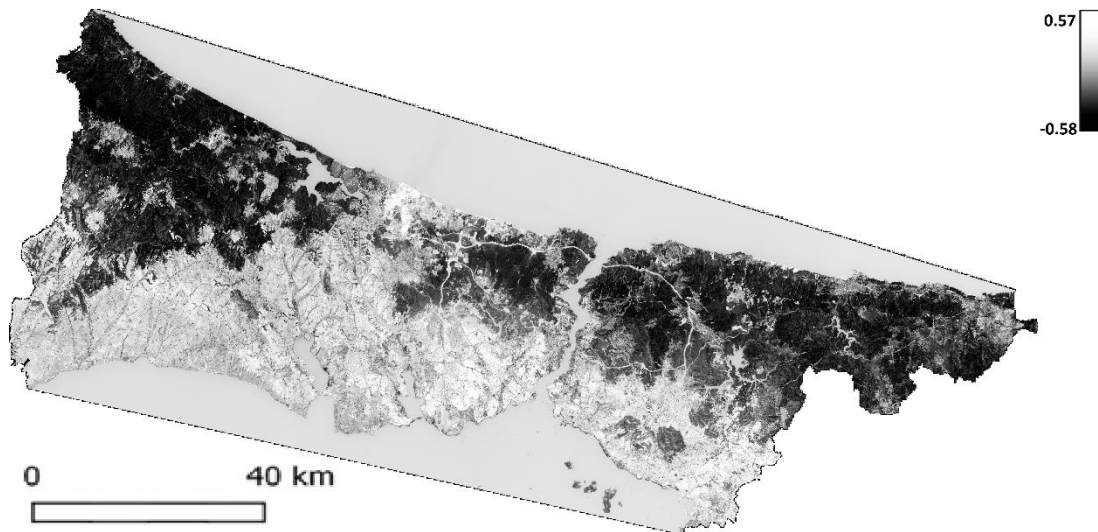


(b)

Figure 5.5 : NDBaI images of Istanbul (a) August 20, 2003 (b) September 06, 2015
 Normalized Difference Bareness Index (NDBaI) is based on significant differences of spectral signature in the nir-infrared (band 5 Landsat5 TM) between the bare-soil and the backgrounds. However, it shows little difference between impervious surface and bare-soil areas in band 5. As seen in Figure 5.5 urban area is slightly dull comparing to bare and farm lands so NDBaI is much effective in distinguishing bare-soil from similarly impervious surface and vegetation.



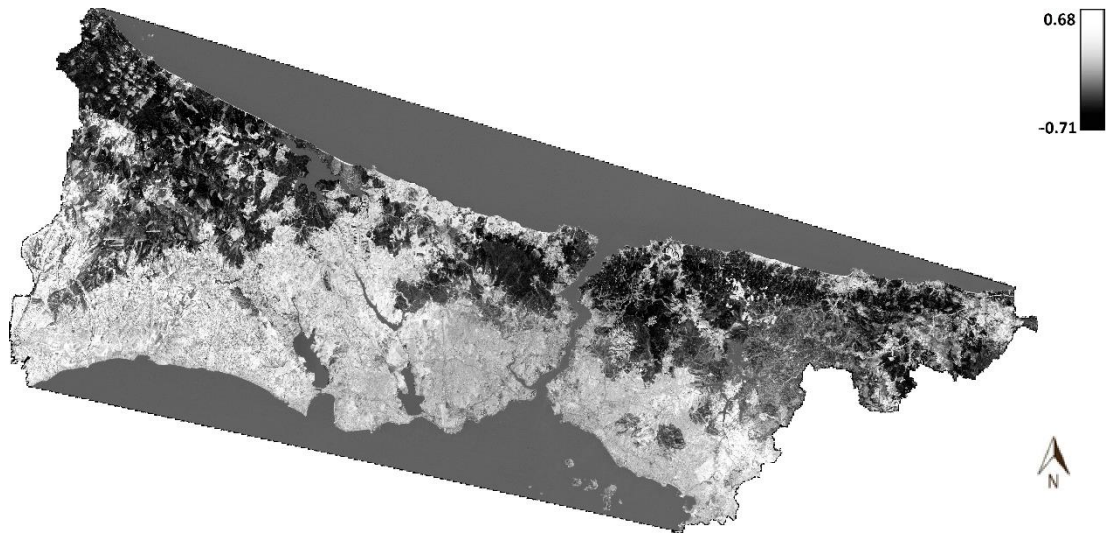
(a)



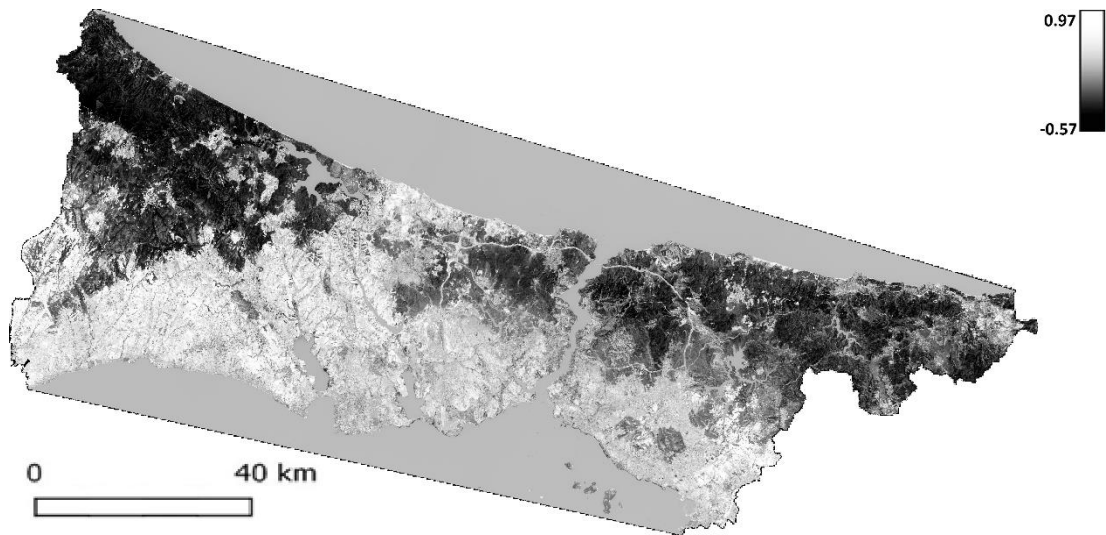
(b)

Figure 5.6 : UI images of Istanbul (a) August 20, 2003 (b) September 06, 2015

With regard to the Figure 5.6, high amount of urban index (UI) value are represented with lighter colours like bright grey colours, where the low UI values are shown with dark colours that illustrates bare land and much darker UI values are classified as vegetation.



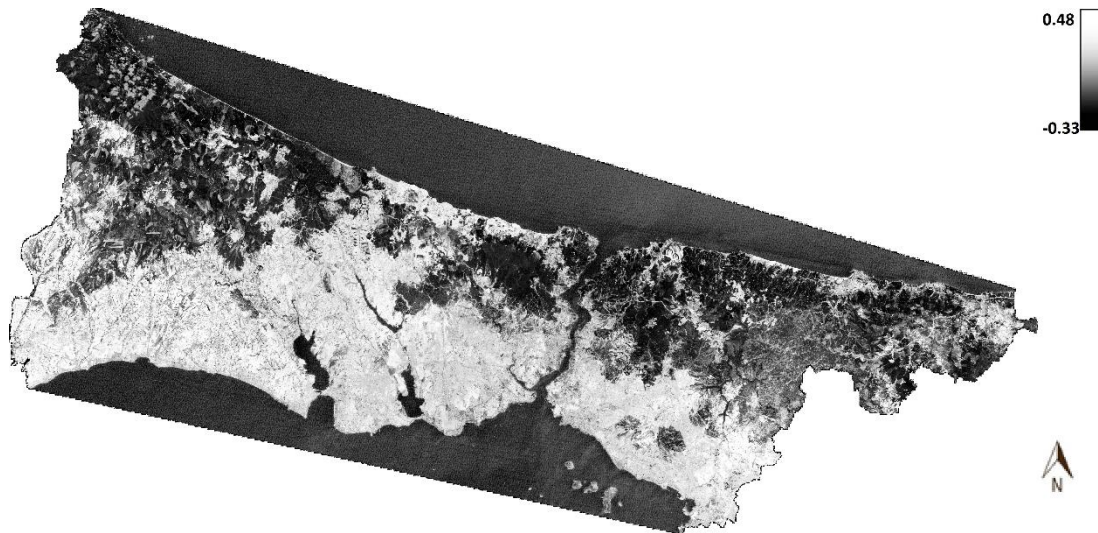
(a)



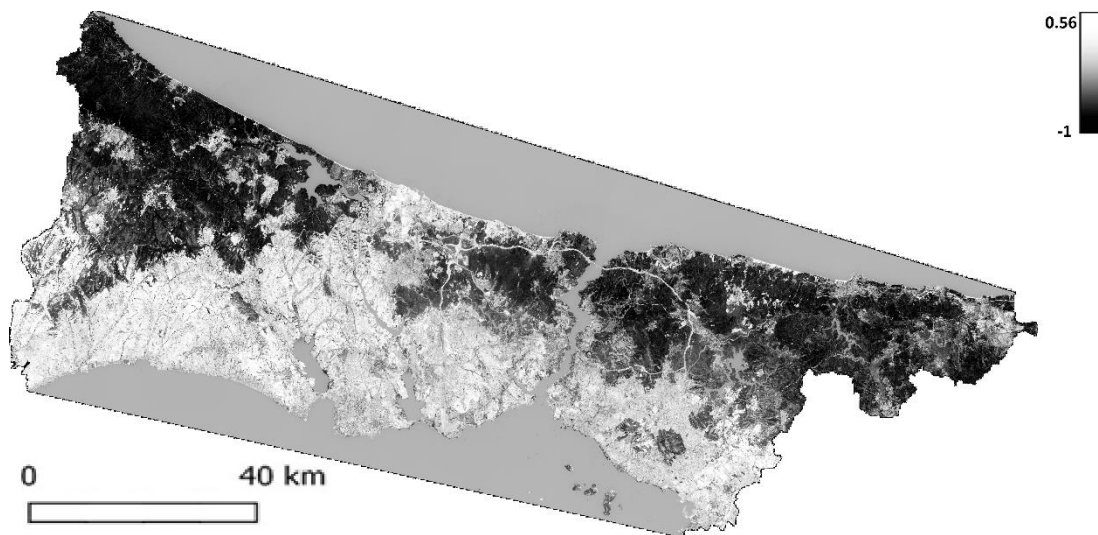
(b)

Figure 5.7 : EBBI images of Istanbul (a) August 20, 2003 (b) September 06, 2015

The transformation of bands 4, 5, and 6 is examined in the EBBI index. EBBI is very effective in distinguishing impervious surface and bare land areas, which is one of the major limitations of applying built-up indices based on remotely sensed data. The use of three infrared channels (NIR, SWIR, and TIR) that reflect different contrasts in detecting impervious surface, bare land, and vegetation areas is responsible for better contrasts of gray levels in Figure 5.7.



(a)



(b)

Figure 5.8 : IBI image of Istanbul (a) August 20, 2003 (b) September 06, 2015

IBI is the only index that is based on other indices and it is made by using SAVI, NDBI and MNDWI indices. IBI is proven to be one of the best urban-bare land indices used on Landsat imagery and shows better results comparing to indices that use just two bands .

The transformation of Landsat bands was examined in this study. This study investigated the mapping of impervious surfaces and bare land areas by index transformation and the results of comparing the relationship between the remote sensing indices and the percentages of impervious surfaces and bare land areas are detailed in this study.

Transforming remote sensing data into an index value required the use of a control index value as a reference index to distinguish the different types of land cover. In this case, the reference was the limit of the index (threshold value) for each type of transformation index, as shown in Table 5.8 and Table 5.9. The limitation of each index was determined by visual interpretation of the data to reference data.

Table 5.8 : Threshold values of the index value for each type of index transformation in determining non-built-up, built-up for August 20, 2003 Landsat 5 TM Image.

| Remote Sensing indices | Impervious Surface | Bare Land |
|--|--------------------|-----------|
| EBBI (Enhanced Built-Up and Bareness Index) | 0.220-0.340 | >0.340 |
| IBI (Index-based Built-Up Index) | 0.315-0.388 | >0.388 |
| NDBI (Normalized Difference Built-Up Index) | 0.220-0.305 | >0.305 |
| UI (Urban Index) | >0.015 | - |
| NDBaI (Normalized Difference Bareness Index) | - | >-0.090 |

Table 5.9 : Threshold values of the index value for each type of index transformation in determining non-built-up, built-up for September 06, 2015 Landsat OLI & TIRS Image.

| Remote Sensing indices | Impervious Surfac | Bare Land |
|--|-------------------|-----------|
| EBBI (Enhanced Built-Up and Bareness Index) | .0100-0.900 | >0.900 |
| IBI (Index-based Built-Up Index) | 0.010-0.120 | >0.120 |
| NDBI (Normalized Difference Built-Up Index) | 0-0.070 | >0.070 |
| UI (Urban Index) | >0 | - |
| NDBaI (Normalized Difference Bareness Index) | - | >-0.310 |

5.4 Mapping Impervious Surface and Bare Land

Mapping and assessing of impervious surface and bare land requires interpretation of remote sensing data with ground truth data. In this study it was assessed the degree of agreement between Landsat imagery and existing google earth maps, assuming that the existing google earth maps were accurate enough to serve as references. The main

reference imagery used in this study are Quick Bird images for 2003 and Wold View-3 for 2015 images.

Then density slicing method was applied in order to classify the impervious surface and bare land. The ranges of density slicing for each index is provided in tables 5.8 and 5.9. This ranges are obtained by comparing the classified image to the reference data and for built-up indices the value under 0 is mostly related to vegetation, forest and farm lands. values near 0 are likely to be water bodies. For impervious surface detection depending on index and the data, the ranges differ and mostly it is around 0.1-0.3. Bare land area appears somehow after impervious surfaces but on some cases it causes mixing except for NDBaI index that bare land is distinguishable even in negative values. After classifying index derived images the impervious surface and bare land areas were determined by each remote sensing transformation index and represented in tables 5.10, 5.11.

Table 5.10 : Impervious surface and bare land areas of each index for August 20, 2003 Landsat 5 TM Image.

| Remote Sensing indices | Impervious Surface(ha) | Bare Land (ha) |
|---|------------------------|----------------|
| EBBI | 121,421 | 63,840 |
| IBI | 117,496 | 38,922 |
| NDBI | 115,808 | 55,338 |
| UI | 48,756 | - |
| NDBaI | - | 67,255 |
| Istanbul Total Area (Except water bodies) | 575,000 | |

Table 5.11 : Impervious surface and bare land areas of each index for September 06, 2015 Landsat 8 OLI & TIRS Image.

| Remote Sensing indices | Impervious Surface(ha) | Bare Land (ha) |
|---|------------------------|----------------|
| EBBI | 137,406 | 38,432 |
| IBI | 132,155.5 | 26,390 |
| NDBI | 131,781 | 30,416.6 |
| UI | 54,682 | - |
| NDBaI | - | 56,508 |
| Istanbul Total Area (Except water bodies) | 575 ,000 | |

Figure 5.9 shows the process of the validation of density slicing classification , class in color blue showing bare land area and red class belongs to impervious surface area and as seen in this image pixels are correctly classified as they are on the reference data.

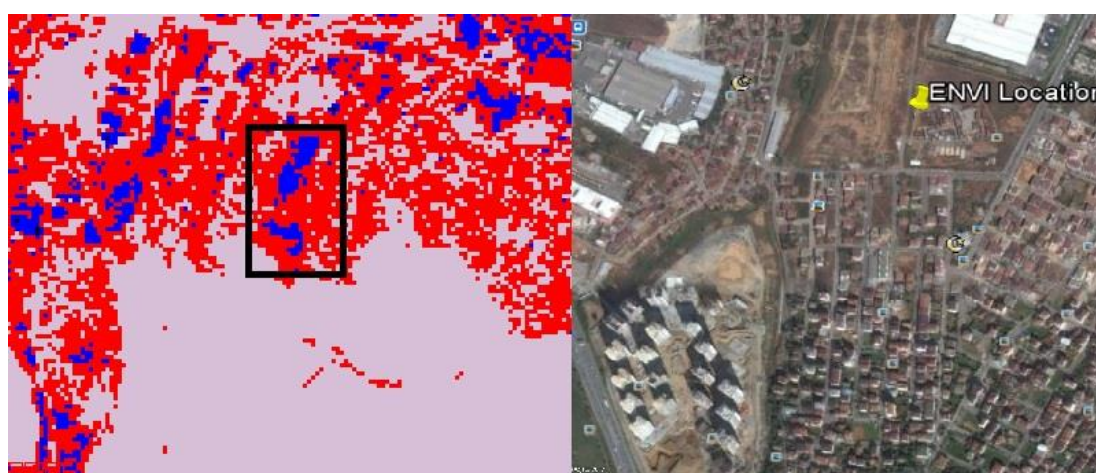


Figure 5.9 : Validation of EBBI index image of August 20, 2003 classified as impervious surface and bare land using Quickbird August 03, 2003 image as reference.

Using the ranges given in Table 5.8 , 5.9 the impervious surface maps of Istanbul are produced and given in Figure 5.10 and 5.11.

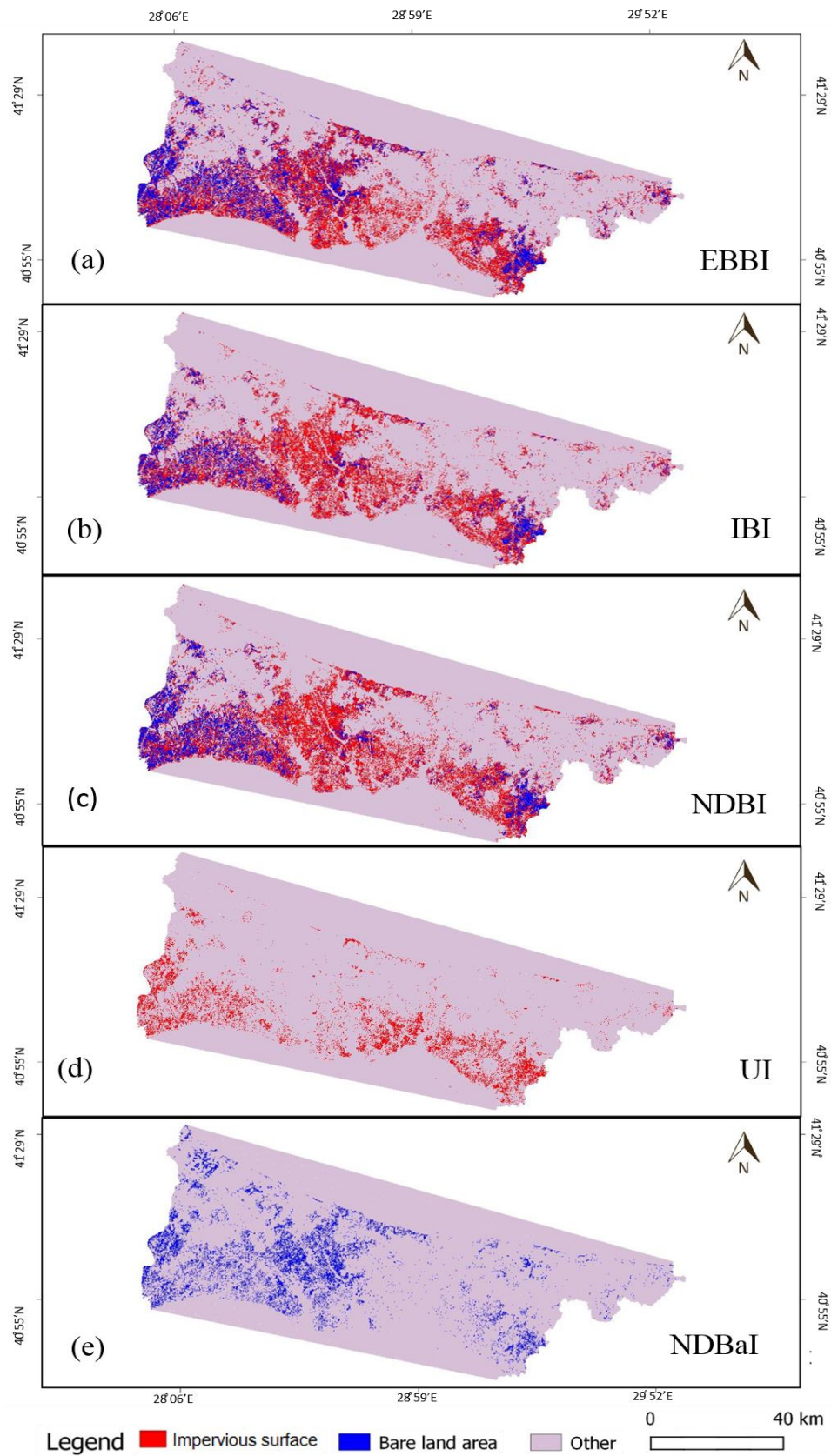


Figure 5.10 : The spatial distribution of impervious surfaces and bare lands is shown for each type of index/remote sensing data transformation for August 20, 2003 Landsat5 TM Image: (a) EBBI, (b) IBI, (c) NDBI, (d) UI, (e) NDBaI

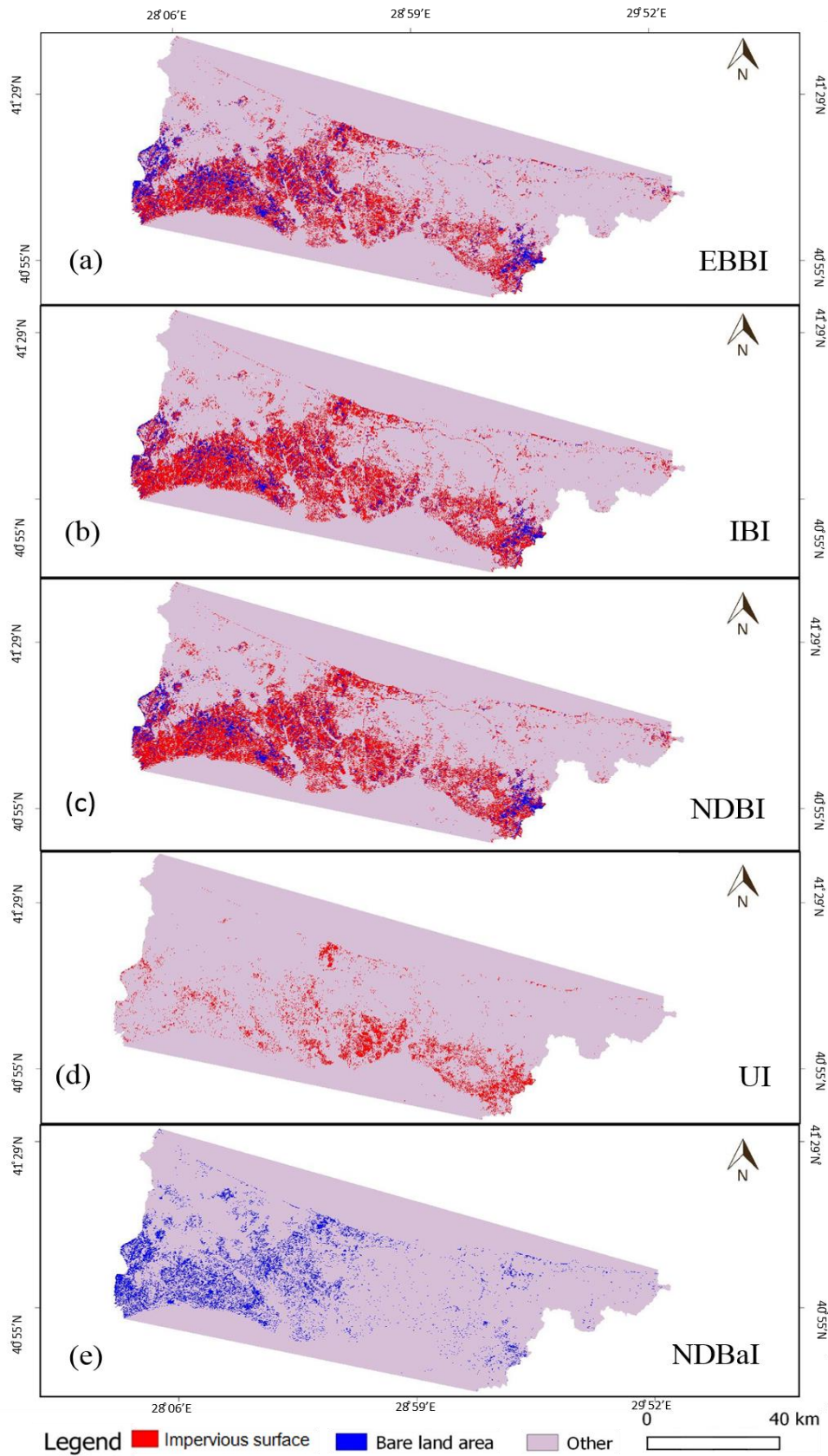


Figure 5.11 : The spatial distribution of impervious surfaces and bare lands is shown for each type of index/remote sensing data transformation for September 06, 2015 Landsat8 OLI & TIRS Image: (a) EBBI, (b) IBI, (c) NDBI, (d) UI, (e) NDBaI

The percentage of impervious surface area confirmed the close relationship between the EBBI results with the percentage of actual impervious surface areas and the results of analysis showed that the total impervious surface area obtained from the EBBI transformation is 137,406 ha. Figure 5.10, and 5.11 show the results of this study and following the EBBI index , IBI index results with 132,155.5 ha area in contrast to other indices show similar pattern as EBBI Index. NDBaI index is very reliable at extracting bare land area and almost show better results than any other index in both 2003 (67,255 ha) and 2015 (56,508 ha) images.

5.5 Accuracy Assessment

Accuracy assessment is a procedure for quantifying how good a job was done by a classifier or how accurate out classification. In thematic mapping from remotely sensed data, the term accuracy is used typically to express the degree of accuracy of a map or classification. Most of the environmental features are extremely dynamic; in most of the cases the temporal and geometric resolution of remotely sensed data cannot cover the dynamic domain of the environmental parameters evolution (atmospheric conditions, soil moisture, and other environmental related phenomena). Accuracy assessment is an important part of classification. It is usually done by comparing the classification product with some reference data that is believed to reflect the true land cover accurately. Sources of reference data include ground truth, higher resolution images, and maps. In this study google earth high resolution imagery was used as the ground truth reference. (Figure 5.12)



Figure 5.12 : Missclassification of bare land as impervious surface in NDBI image Landsat5 TM August 20, 2003 in contrast to Quickbird August 03, 2003 image.

In Figure 5.13 Ataturk Airport is shown and the ability of each index in extracting land cover is tested. Ataturk airport has 1165 ha total area and 965 ha impervious surface area.

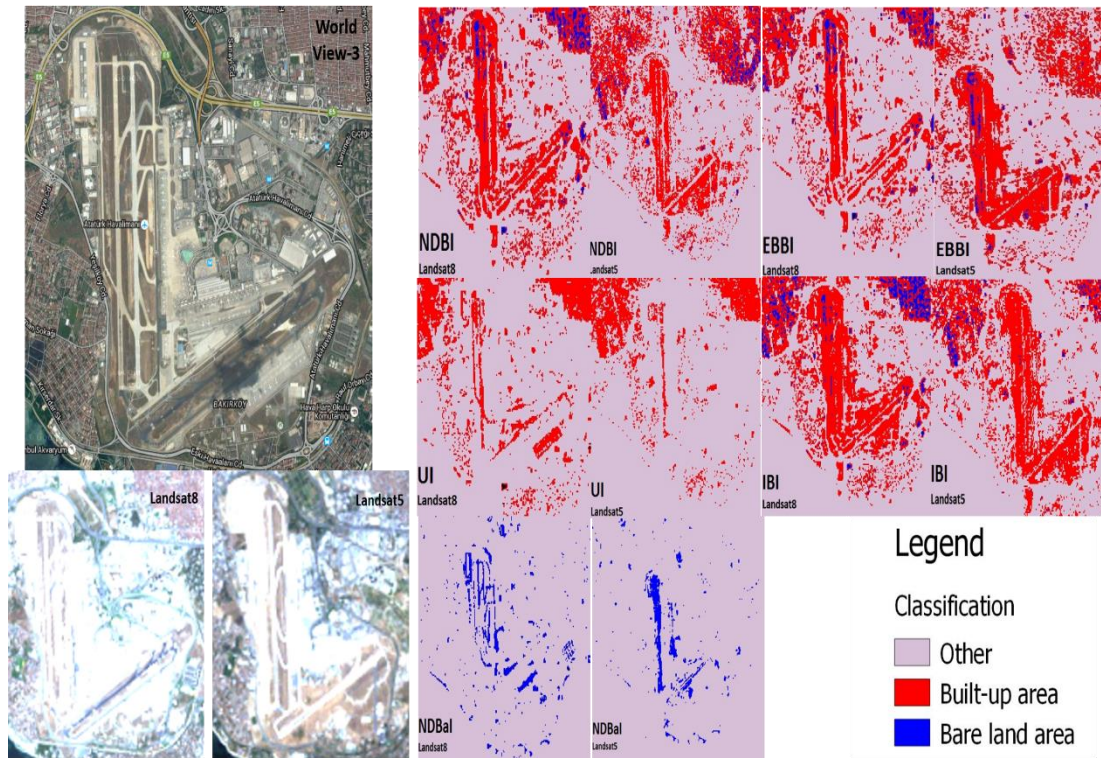


Figure 5.13 : Ataturk airport land cover extraction by urban indices

As shown in Figure 5.13, due to mixture of land cover around Istanbul Ataturk Airport each index presents impervious surfaces distinctly from other indices. Table 5.12 and 5.13 provide impervious surface area of Istanbul Ataturk airport using built-up and bare land indices. The EBBI index is showing better results on landsat 5 TM data and IBI index has promising results on landsat 8 OLI & TIRS data comparing to other urban indices.

Table 5.12 : Impervious surface and bare land area of farmland for each index for August 20, 2003 Landsat5 TM Image.

| Remote Sensing indices | Impervious Surface(ha) | Bare Land (ha) |
|------------------------|------------------------|----------------|
| EBBI | 763 | 62 |
| IBI | 614 | 15 |
| NDBI | 387 | 11 |
| UI | 76 | - |
| NDBaI | - | 147 |

Table 5.13 : Impervious surface and bare land area of farmland for each index for September 06, 2015 Landsat8 OLI & TIRS Image.

| Remote Sensing indices | Impervious Surface(ha) | Bare Land (ha) |
|------------------------|------------------------|----------------|
| EBBI | 530 | 74 |
| IBI | 715 | 49 |
| NDBI | 588 | 67 |
| UI | 92 | - |
| NDBaI | - | 173 |

A farmland area west of Istanbul was selected to examine the accuracy of each index on extracting bare land (Figure 5.13, Table 5.16 & 5.17)

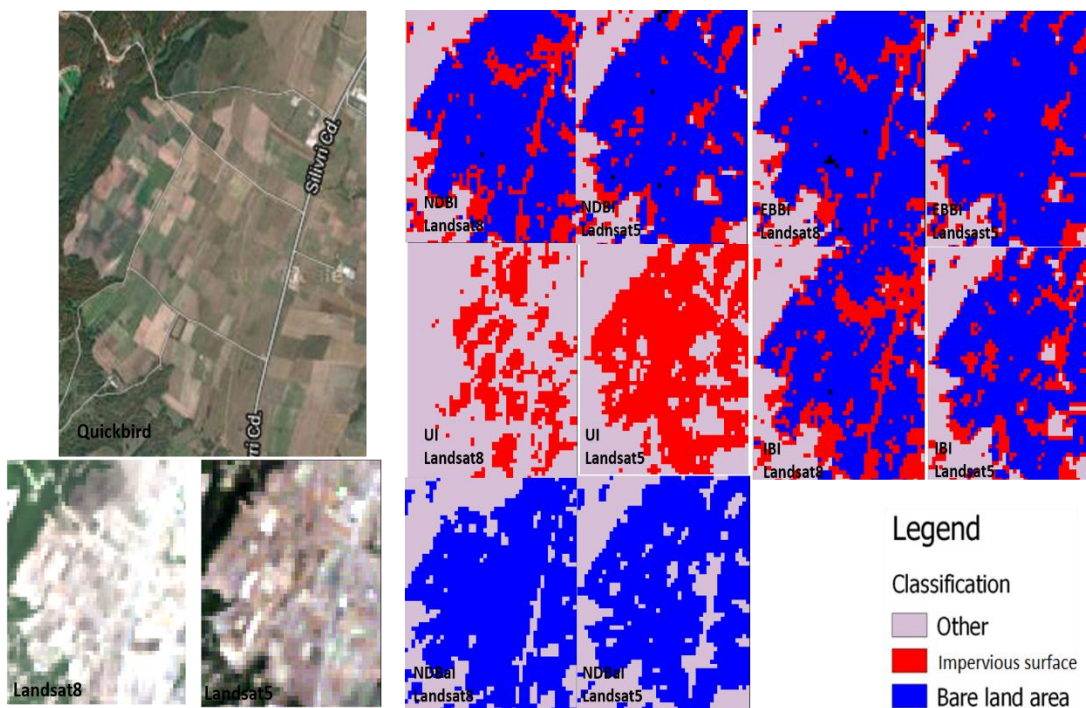


Figure 5.14 : Farmland west of Istanbul (Quickbird)

Table 5.14 : Impervious surface and bare land area of farmland of each index for August 20, 2003 TM Image.

| Remote Sensing indices | Impervious Surface(ha) | Bare Land (ha) |
|------------------------|------------------------|----------------|
| EBBI | 3.50 | 202 |
| IBI | 4 | 185 |
| NDBI | 3.50 | 197 |
| UI | 168 | - |
| NDBaI | - | 190 |
| Total Area | 4.50 | 210 |

Table 5.15 : Impervious surface and bare land areas of farmland of each index for September 06, 2015 Landsat OLI & TIRS Image.

| Remote Sensing indices | Impervious Surface(ha) | Bare Land (ha) |
|------------------------|------------------------|----------------|
| EBBI | 6 | 194 |
| IBI | 26 | 171 |
| NDBI | 17 | 188 |
| UI | 69 | - |
| NDBaI | - | 182 |
| Total Area | 4.50 | 210 |

Another type of urban feature is man made roads. An asphalt road by the Buyukcavuslu in silivri district was selected to assess the capability of each index on extracting this type of impervious surface (Figure 5.15, Table 5.16 & 5.17).

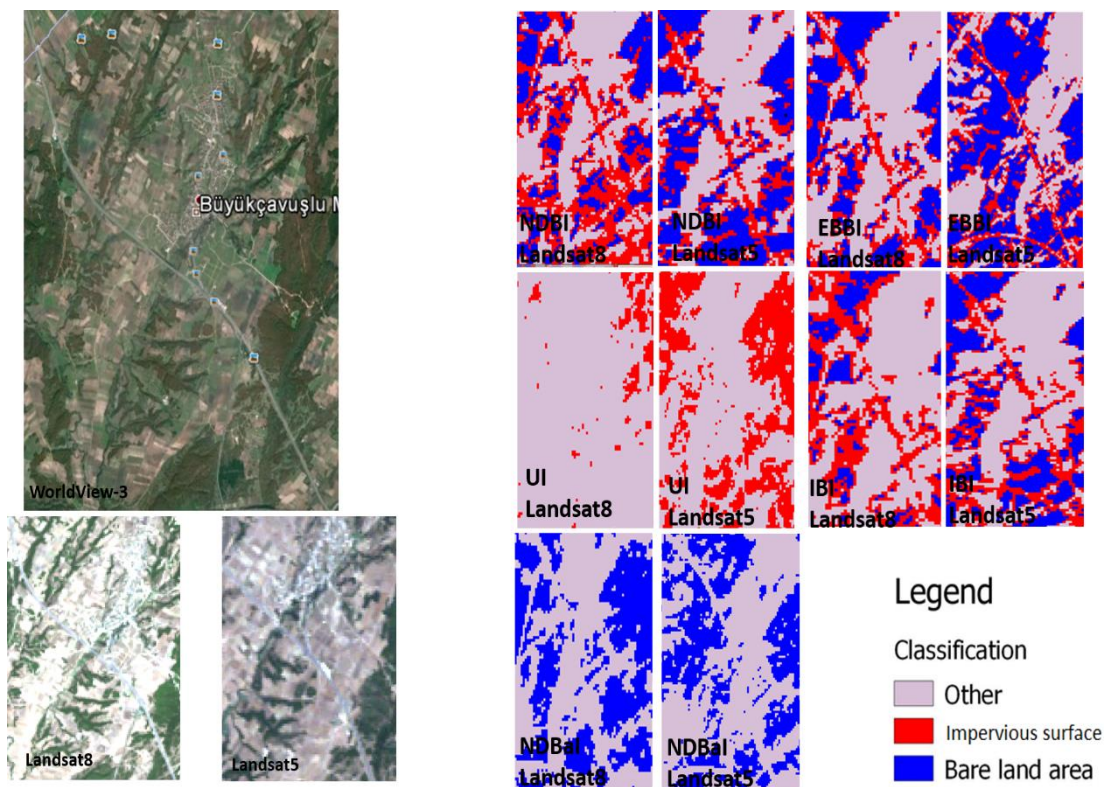


Figure 5.15 : Road by the Buyukcavuslu (WorldView-3)

Table 5.16 : Length of road of each index for August 20, 2003 Landsat5 TM Image.

| Remote Sensing indices | Impervious Surface Area(km) | Bare Land (km) |
|------------------------|-----------------------------|----------------|
| EBBI | 6.04 | - |
| IBI | 6.01 | - |
| NDBI | 5.20 | - |
| UI | 2.40 | - |
| NDBaI | - | - |
| Total Length | 6.12 | - |

Table 5.17 : Length of road of each index for September 06, 2015 Landsat8 OLI & TIRS Image.

| Remote Sensing indices | Impervious Surface Area(km) | Bare Land (km) |
|------------------------|-----------------------------|----------------|
| EBBI | 6.02 | - |
| IBI | 6.05 | - |
| NDBI | 5.35 | - |
| UI | 1.60 | - |
| NDBaI | - | - |
| Total Length | 6.12 | - |

According to Congalton (1988) samples are selected in a order to yield too many samples in large impervious surfaces and too few samples in smaller areas. As a rule of thumb Congalton (1991) recommends at least 50 samples per class and if the area exceeds 500 km² then at least 75-100 samples should be chosen per class. Istanbul having more than 5,750 km² urban area and having just 3 classes such as impervious surface, bare land, others; therefore random sample points was selected for each class and to accomplish a better accuracy, google maps high resolution imagery (Quickbird and World View-3) was used as a reference date. Others category includes forest areas, water surfaces and vegetated areas. Result of the accuracy assessment is provided in (Table 5.18).

Table 5.18 : Accuracy assessment result table.

| Date | Index | Classess | Overall Accuracy | Kappa |
|-------------|--------------|--------------------|-------------------------|--------------|
| 2003 | | | | |
| | EBBI | Impervious Surface | 89% | 93.6% |
| | | Bare Land | 93% | 85% |
| | | Others | 87% | 90.6% |
| | | Overall | 86% | 79% |
| | IBI | Impervious Surface | 84% | 85.7% |
| | | Bare Land | 78% | 84.8% |
| | | Others | 92% | 84% |
| | | Overall | 84.6% | 77% |
| | NDBI | Impervious Surface | 73% | 80% |
| | | Bare Land | 72% | 71% |
| | | Others | 81% | 75% |
| | | Overall | 75.3% | 63% |
| | UI | Impervious Surface | 90% | 83% |
| | | Bare Land | 86% | 77% |
| | | Others | 70% | 86.4 |
| | | Overall | 82% | 73% |
| | NDBaI | Impervious Surface | 75% | 87% |
| | | Bare Land | 88% | 76.5% |
| | | Others | 80% | 89% |

| | | | | |
|-------------|--|--------------------|-------|-------|
| | | Overall | 81% | 71.5% |
| 2015 | | | | |
| EBBI | | Impervious Surface | 87% | 83% |
| | | Bare Land | 83% | 87% |
| | | Others | 90% | 90% |
| | | Overall | 86% | 80% |
| IBI | | Impervious Surface | 81% | 83.5% |
| | | Bare Land | 89% | 86% |
| | | Others | 92% | 92% |
| | | Overall | 87.3% | 81% |
| NDBI | | Impervious Surface | 78% | 79% |
| | | Bare Land | 86% | 75% |
| | | Others | 79% | 91% |
| | | Overall | 81% | 71.5% |
| UI | | Impervious Surface | 69% | 92% |
| | | Bare Land | 87% | 93.5% |
| | | Others | 95% | 72% |
| | | Overall | 83.6% | 75.5% |
| NDBaI | | Impervious Surface | 86% | 95% |
| | | Bare Land | 92% | 85% |
| | | Others | 93% | 91% |
| | | Overall | 90.3% | 85.5% |

Classification based on Landsat 8 OLI & TIRS (September 06,2015) imagery show better results , NDBaI index has a higher precision due to just being able to detect only bare land area and we can observe that EBBI and IBI have the highest accuracy among the built-up and bare land indices. Overall EBBI index has the highest accuracy results in both data sets.

6. CONCLUSIONS AND RECOMMENDATIONS

Determination of impervious surfaces and bare lands is very important for sustainable management and planning of urban areas such as Istanbul. Urban remote sensing indices are generally used to extract impervious surface and bare land areas based on spectral values with acceptable level of accuracy. High degree of homogeneity in the land-use categories, specially in urban areas makes it difficult to achieve high accuracy levels. Bare-soil plays an important role in the ecosystem. It could be the indicator of urban expansion. It is very important to monitor the bare-soil areas.

In this thesis, Landsat 5 TM and Landsat 8 OLI & TIRS data obtained in two different dates (August 20, 2003 and September 06, 2015) were used for detecting impervious surface and bare land area in Istanbul.

Overall, five spectral indices, including the most powerful indices in the literature were taken into consideration. Enhanced Built-up and Bareness Index (EBBI), Normalised Difference Built-Up Index (NDBI), Index-based Built-Up Index (IBI), Urban Index (UI), Normalised Difference Bareness Index (NDBaI) are founded as the most useful ones.

The application of TIR channels, which exhibit high emissivity in impervious surface, is one of the reasons that indices examining thermal band are better indices for distinguishing between classes of land use. The high emissivity in impervious surface areas is caused by the types of materials that are predominately found in these areas, such as roofing and building materials. In contrast, the emissivity of bare soil is determined by the level of soil moisture and by the mineral constituents of the soil. Impervious surface areas exhibit higher heat conductivity than bare soil areas, resulting in the higher emissivity and albedo values of thermal infrared waves in impervious surfaces relative to bare soil areas.

Main conclusions which are drawn from this study, are summarized below:

Heterogeneity embedded within the nature of Istanbul makes the task of reliable and accurate mapping of impervious surfaces and bare lands more difficult.

The more simultaneously collected ground truth data with remotely sensed data are used, the better accuracy can be observed to determine impervious surfaces and bare lands in heterogeneous urban areas.

Most of the urban indices are generated based on homogeneous cities therefore it is suggested to investigate the use of urban indices on heterogeneous areas in future studies.

Besides the importance of using thermal bands in examining urban area, the EBBI index is still a new index and it is crucial to investigate more about this index using Landsat 8 OLI & TIRS data.

Another issue is finding proper Landsat 8 OLI & TIRS imagery without clouds in the study area. Istanbul with a Mediterranean weather usually clouds are expected to appear over the city. Although Landsat 8 being operational for more than three years all over the world, hence having 16 days temporal resolution makes it hard to acquire desired data.

One other problem is the spatial resolution of Landsat 5 TM and Landsat 8 OLI & TIRS satellites (30 meters). The higher resolution makes the sampling easier in the image data. In this study, the sampling of impervious surface area measurements could be easier in the case of using higher spatial resolution.

Besides the spatial resolution, spectral resolution also plays an important role for better interpretation of the satellite imageries. Hyperspectral sensors can be a better solution, since they capture a large amount of narrow bands which referred to as a high spectral; however, multispectral satellites such as Landsat 5 and 8 capture the small number of wide bands. High spectral resolution makes it easy to distinguish between features spectrally in the image. Since impervious surface area in the infrared and thermal portion of electromagnetic spectrum has a strong reflectance that enables better detection, the more these bands are available, the impervious surface area would be detected more precisely. As a result, using the hyperspectral satellites in impervious surface area detection could be more effective than multispectral satellites.

After comparing the results of indices, NDBaI index is considered to have promising results for bare soil but overall EBBI index is chosen to be the more precise transformation to make the impervious surface and bare land map of Istanbul.

As a conclusion, some issues named above should be considered as recommendations for the future studies to be planned on this topic.

7. REFERENCES

- A modern Approach to Regression with R.* (2009). Sheather, S., Springer Science & Business Media.
- Arnold, C. L. Jr., and Gibbons, C. J.** (1996). Impervious surface coverage: The emergence of a key environmental indicator. *Journal of the American Planning Association*, 62, 243–258.
- As-Syakur, A. R., Adnyana, I., Arthana, I. W., and Nuarsa, I. W.** (2012). Enhanced Built-Up and Bareness Index (EBBI) for mapping built-up and bare land in an urban area. *Remote Sensing*, 4(10), 2957-2970.
- Ayazli, I. E.** (2011). *Simulation model of urban sprawl driven by transportation networks: 3rd Bosphorus bridge example.* (Ph.D. Thesis). Yildiz Technical University, Istanbul.
- Balçık, F. B.** (2013). Determining the impact of urban components on land surface temperature of Istanbul by using remote sensing indices. *Environmental monitoring and assessment*, 186(2), 859-872.
- Bellard, C., Bertelsmeier, C., Leadley, P., Thuiller, W., and Courchamp, F.** (2012). Impacts of climate change on the future of biodiversity. *Ecology letters*, 15(4), 365-377.
- Braun, M., & Herold, M.** (2004). Mapping imperviousness using NDVI and linear spectral unmixing of ASTER data in the Cologne-Bonn region (Germany). *Proceedings of the SPIE 10th international symposium on remote sensing*, Barcelona, Spain, 8–12 Sept 2003.
- Brun, S. E., and Band, L. E.** (2000). Simulating runoff behavior in an urbanizing watershed. *Computers, Environment and Urban Systems*, 24, 5–22.
- Burak, S., Doğan, E. and Gazioğlu, C.** (2004). Impact of urbanization and tourism on coastal environment. *Ocean and Coastal Management*, 47, pp.515–527.
- Borges, J. S.** (2008). *Bayesian hyperspectral image segmentation with discriminative class learning.* University of Porto, Porto, Portuguese.
- Chen, X-L., Zhao, H-M., Li, P-X., and Yin, Z-Y.** (2006). Remote sensing image-based analysis of the relationship between urban heat island and land use/cover changes. *Remote Sensing of Environment*, 104, 133–146.

- Chen, J., Zhu, X., Vogelmann, J. E., Gao, F., and Jin, S.** (2011). A simple and effective method for filling gaps in Landsat ETM⁺ SLC-off images. *Remote Sensing of Environment*, 115,4. p: 1053-64.
- Coban, H.O., Koc, A. and Eker, M.** (2010). Investigation on changes in complex vegetation coverage using multi-temporal landsat data of Western Black sea region - A case study. *Journal of Environmental Biology*, 31, pp.169–178.
- Congalton, R.** (1988) A comparison of sampling schemes used in generating error matrices for assessing the accuracy of maps generated from remotely sensed data. *Photogrammetric Engineering and Remote Sensing*, 54(5):593–600.
- Congalton, R.** (1991) A Review of Assessing the Accuracy of Classifications of Remotely Sensed Data. *Remote Sensing of Environment*, 37:35–46.
- Elvidge, C. D., Tuttle, B. T., Sutton, P. C., Baugh, K. E., Howard, A. T., Milesi, C., and Nemani, R.** (2007). Global distribution and density of constructed impervious surfaces. *Sensors*, 7(9), 1962-1979.
- Encyclopedia of Geographic Information Science.* (2008). Karen, K. K.
- Encyclopedia of geographic information science.* (2008). Kemp, K., Sage.
- ERDAS, Inc.** (1999). ERDAS Field Guide, 5th edition, ERDAS Inc., Atlanta, GA.
- ERDAS, Inc.** (2014). Fundamentals of ERDAS Imagine, Atlanta, GA.
- Flanagan, M.** (2001). Subpixel Impervious Surface Mapping. *Proceedings of the ASPRS Annual Conference*, , St.Louis, Missouri, USA, April 23-27, 2001.
- Foody, G. M.** (2002). Status of land cover classification accuracy assessment. *Remote sensing of environment*, 80(1), 185-201
- Fundamentals of remote sensing and airphoto interpretation.* (1992). Avery, T. E., and Berlin, G. L.
- Geymen, A. and Baz, I.** (2008). Monitoring urban growth and detecting land-cover changes on the Istanbul metropolitan area. *Environmental monitoring and assessment*, 136(1-3), pp.449–459.
- Goksel, C., Musaoglu, N., Gurel, M., Ulugtekin, N., Tanik, A., and Seker, D. Z.** (2006). Determination of land-use change in an urbanized district of Istanbul via remote sensing analysis. *Fresenius Environmental Bulletin*, 15(8a), 798–805.
- Hasanlou M., and Mostofi N.** (2015). Investigating Urban Heat Island Estimation and Relation between Various Land Cover Indices in Tehran City Using Landsat 8 Imagery. *1st International Electronic Conference on Remote Sensing*, 22 June-05 July 2015.

- Harris, S., Veraverbeke, S., and Hook, S.** (2011). Evaluating spectral indices for assessing fire severity in chaparral ecosystems (Southern California) using MODIS/ASTER (MASTER) airborne simulator data. *Remote sensing*, 3(11), 2403-2419.
- Hurd, J. D., and Civco, D. L.** (2004). Temporal characterization of impervious surfaces for the State of Connecticut. *ASPRS Annual Conference Proceedings*, Denver, Colorado, May 2004 (Unpaginated CD-ROM).
- Introduction to the physics and techniques of remote sensing (Vol. 28).* (2006). Elachi, C., and Van Zyl, J. J., John Wiley & Sons.
- Jia, K., Wei, X., Gu, X., Yao, Y., Xie, X., and Li, B.** (2014). Land cover classification using Landsat 8 operational land imager data in Beijing, China. *Geocarto International*, 29(8), 941-951.
- Fundamentals of remote sensing.* (2005). Joseph, G., Universities Press.
- Kaya, S. and Curran, P.J.** (2006). Monitoring urban growth on the European side of the Istanbul metropolitan area: A case study. *International Journal of Applied Earth Observation and Geoinformation*, 8(1), pp.18–25.
- Kaya, S., Osgouei, P. E., Alganci, U., Seker, D. Z. and Gazioglu, C.** (2015). Evaluation of Vegetation Density Changes in Suburban Area: A Case Study of Istanbul Metropolitan Area. *ACRS 2015: The 36 th Asian Conference on Remote Sensing “Fostering Resilient Growth in Asia”*, Quezon City, Metro Manila, Philippines, 19-23 October 2015, pp.1-2
- Kurt, S.** (2012). Land Use Changes in Istanbul’s Marmara Sea Coastal Regions Between 1987 and 2007. *Middle-East Journal of Scientific Research*, 11 (11): 1584-1590, 2012
- Landsat 7 Science Data Users Handbook.**
http://ltpwww.gsfc.nasa.gov/IAS/handbook/handbook_toc.html. date retrieved 10.05.2016.
- Landsat, U. S. G. S. 8 (L8).** (2016) Data Users Handbook Version 1.0.
- Masek, J.G., F.E. Lindsay and Goward,** (2000). Dynamics of urban growth in the Washington DC metropolitan area, 1973-1996, from Landsat observations. *International Journal of Remote Sensing*, 21(18): pg.3473-3486.
- Merriam-Webster's Collegiate Dictionary Thesaurus : Electronic Edition, Version I.* (1994). Merriam Webster.
- Musaoglu, N., Tanik, A., and Kocabas, V.** (2005). Identification of Land-Cover Changes Through Image Processing and Associated Impacts on Water Reservoir Conditions. *Environmental Management*, Vol. 35, No. 2, pp. 220–230

- Musaoglu, N., Gurel, M., Ulugtekin, N., Tanik, A., and Seker, D. Z.** (2006). Use of remotely sensed data for analysis of land-use change in a highly urbanized district of mega city, Istanbul. *Journal of Environmental Science and Health, Part A*, 41(9), 2057-2069.
- Mundhe, N. N., and Jaybhaye, R. G.** (2014). Impact of urbanization on land use/land covers change using Geo-spatial techniques. *International journal of geomatics and geosciences*, Volume 5, No 1, 2014
- Principles of remote sensing. Longman Inc.* (1985). Curran, P. J.
- Remote sensing and image interpretation.* (2014). Lillesand, T., Kiefer, R. W., and Chipman, J., John Wiley & Sons.
- Remote Sensing of the Environment: An Earth Resource Perspective (2nd Edition).* (2009). Jensen, J. R., Pearson Education India.
- Remote sensing: models and methods for image processing.* (2006). Schowengerdt, R. A., Academic press.
- Rikimaru, A., and Miyatake, S.** (1997). Development of Forest Canopy Density Mapping and Monitoring Model using Indices of Vegetation, Bare soil and Shadow. *In Proceeding of the 18th Asian Conference on Remote Sensing (ACRS) 1997*, Kuala Lumpur, Malaysia, 20–25; p. 3.
- Sanli, F. B., Balcik, F. B., and Goksel, C.** (2008). Defining temporal spatial patterns of mega city Istanbul to see the impacts of increasing population. *Environmental monitoring and assessment*, 146(1-3), 267-275.
- Schueler, T. R.** (1994). The Importance of Imperviousness. *Watershed Protection Techniques*, vol. 1, no. 3.
- Singh, R. P., and Sirohi, A.** (1995). Spectral Reflectance Properties of Different Types of Built-up Surfaces. *Journal of Aerospace Engineering*, Vol. 8, No. 1, pp. 25-31
- Sleavin, W. J.** (1999). *Measuring Impervious Surfaces in Connecticut Using Planimetric GIS Data.* (Thesis). Department of Natural Resource Management and Engineering, University of Connecticut, Storrs, CT.
- Sleavin, W. J., Civco, D. L., Prisloe, S., and Giannotti, L.** (2000). Measuring impervious surfaces for non-point source pollution modeling. *In Proceedings of the ASPRS 2000 Annual Convention.* (pp. 22-26).
- Song, D. X., Huang, C., Sexton, J. O., Channan, S., Feng, M., and Townshend, J. R.** (2015). Use of Landsat and Corona data for mapping forest cover change from the mid-1960s to 2000s: Case studies from the Eastern United States and Central Brazil. *ISPRS Journal of Photogrammetry and Remote Sensing*, 103, 81-92.

- Stankowski, S. J.** (1972). Population Density as an Indirect Indicator of Urban and Suburban Land-Surface Modifications. *U.S. Geological Survey Professional Paper*, 800-B.
- Turner, B., Skole, D., Sanderson, S., Fischer, G., Fresco, L., and Leemans, R.** (1995). Land-use and land-cover change In International Geosphere-Biosphere Programme (Report No. 35). Stockholm.
- Van Niel, T. G.** (1995). Classification of vegetation and analysis of its recent trends at Camp Williams, Utah using remote sensing and geographic information system techniques. Utah State University. Department of Watershed Science.
- Url-1** <http://www.gisresources.com/an-insight-to-ndvi_2/>, date retrieved 10.04.2016.
- Url-2** <<http://www.mdcoastalbays.org/bayissues-stormwater-management>>, date retrieved 18.05.2016.
- Url-3** <<http://www.shariqa.com/waves%20around%20us.htm>>, date retrieved 15.04.2016.
- Url-4** <http://en.wikipedia.org/wiki/Remote_sensing>, date retrieved 15.04.2016.
- Url-5** <<http://www.turkstat.gov.tr>>, date retrieved 26.05.2016
- Weng, Q.** (2008). Remote Sensing of Impervious Surfaces: An Overview. In Remote Sensing of Impervious Surfaces.
- Weng, Q.** (2012). Remote sensing of impervious surfaces in the urban areas: Requirements, methods, and trends. *Remote Sensing of Environment*, 117, 34-49.
- Xu, H.** (2007). Extraction of Urban Built-up Land Features from Landsat Imagery Using a Thematic-oriented Index Combination Technique. *Photogrammetric Engineering Remote Sensing*, Vol. 73, No. 12, pp. 1381-1391
- Xu, H.** (2008). A new index for delineating built-up land features in satellite imagery. *Int. J. Remote Sens*, 2008, 29, 4269–4276.
- Yitong, J., Fu, P., and Weng, Q.** (2015). Assessing the Impacts of Urbanization-Associated Land Use/Cover Change on Land Surface Temperature and Surface Moisture: A Case Study in the Midwestern United States. *Remote Sens*, 2015, 7, 4880-4898; doi:10.3390/rs70404880
- Yuan, F., Sawaya, K. E., Loeffelholz, B. C., and Bauer, M. E.** (2005). Land cover classification and change analysis of the Twin Cities (Minnesota) Metropolitan Area by multitemporal Landsat remote sensing. *Remote sensing of Environment*, 98(2), 317-328.

- Zha, Y., Gao, J., and Ni, S.** (2003). Use of normalized difference built-up index in automatically mapping urban areas from TM imagery. *Int. J. Remote Sens*, 24, 583–594.
- Zhao, H. M. and Chen, X. L.** (2005). Use of Normalized Difference Bareness Index in Quickly Mapping Bare Areas from TM/ETM+. *In Proceedings of 2005 IEEE International Geoscience and Remote Sensing Symposium, Seoul, Korea, 25–29; Volume 3*, pp. 1666-1668.

CURRICULUM VITAE



Name Surname : Kaveh KHORSHID

Place and Date of Birth : Iran , 01.09.1984

E-Mail : kaveh.khorshid@yahoo.com

B.Sc. : 2011, Urmia University, Civil Engineering Department